Title page

Magnetic Anomalies in Extensional Detachments: The Xistral Tectonic Window of the Lugo Dome (NW Spain)

Authors:

José R. Martínez Catalán
Departamento de Geología, Universidad de Salamanca, 37008 Salamanca, Spain.
E-mail: jrmc@usal.es

Puy Ayarza
Departamento de Geología, Universidad de Salamanca, 37008 Salamanca, Spain.
E-mail: puy@usal.es

Fernando Álvarez Lobato
Departamento de Geología, Universidad de Salamanca, 37008 Salamanca, Spain.
E-mail: fernando@usal.es

Juan José Villalaín
Laboratorio de Paleomagnetismo, Departamento de Física, Universidad de Burgos, 09006 Burgos, Spain.
E-mail: villa@ubu.es

Manuela Durán Oreja
Departamento de Geología, Universidad de Salamanca, 37008 Salamanca, Spain.
E-mail: manuduor@usal.es

Manuel Martín Paramio
Departamento de Geología, Universidad de Salamanca, 37008 Salamanca, Spain.
E-mail: manu_martin92@hotmail.es

Silvia Rodríguez Gómez
Departamento de Geología, Universidad de Salamanca, 37008 Salamanca, Spain.
E-mail: silviarodriguez.geo@gmail.com

Corresponding author: J.R. Martínez Catalán. Phone: +34 630279290; Fax: +34 923294514.
E-mail: jrmc@usal.es

Magnetic Anomalies in Extensional Detachments: The Xistral Tectonic Window of the Lugo Dome (NW Spain)

José R. Martínez Catalán[1], Puy Ayarza[1], Fernando Álvarez Lobato[1], Juan José Villalaín[2], Manuela Durán Oreja[1], Manuel Martín Paramio[1], and Silvia Rodríguez Gómez[1]

[1]*Departamento de Geología, Universidad de Salamanca, 37008 Salamanca, Spain,*
[2]*Laboratorio de Paleomagnetismo, Departamento de Física, Universidad de Burgos, 09006 Burgos, Spain*

Corresponding author: J.R. Martínez Catalán. Tel.: +34 670556355; fax: +34 923294514

E-mail address: jrmc@usal.es

Abstract The Eastern Galicia Magnetic Anomaly (EGMA) is a conspicuous feature of the aeromagnetic map of Iberia which structurally overlaps the Lugo and Sanabria domes, two spatially linked late Variscan extensional structures that delineate a segment of the Ibero-Armorican Arc. In the northern part of the Lugo Dome, the Xistral Tectonic Window exposes a deep section of the continental crust which includes several extensional detachments and associated shear zones. The aim is to check whether or not there is a correlation between the extensional process and the EGMA. A map of the magnetic anomaly of the Xistral Tectonic Window acquired on land improves the resolution of the aeromagnetic data and shows that the EGMA is actually composed by several shorter wavelength anomalies reaching amplitudes up to 1214 nT. Their location in relation to outcropping rocks and structures, together with 2D modeling shows a conspicuous link between the anomalies and the extensional detachments. On a larger scale, the EGMA forms the northern part of a largeanomaly occupying the core of the Central Iberian Arc. This anomaly can be related to extension caused by gravitational collapse of the thickened Variscan crust, implying that like the EGMA, local anomalies might reflect extensional structures, many of which may remain buried. Our study may shed light on the origin of magnetic anomalies in other gneiss domes as it shows that they can be related with the doming process instead of being inherited from older rocks presently outcropping at the core of the domes.

1. Introduction

Gneiss domes are common major structures of orogens. The original definition of *Eskola* [1949] of a core of migmatites, granites and other high-grade metamorphic rocks overlain by metamorphic rocks of lesser grade has been expanded to any domal structure cored by gneisses and granitoids. A gneissic basement cropping out in a dome surrounded by sediments and/or volcanic rocks may be included in this category. Gneiss domes may result from very different processes. They may form by constrictional buckling or interference of large buckle folds [*Yin*, 2004], with large wavelengths favored by contrasting competence. They can be fault-bend folds in thrust belts involving cover and basement [*Fisher and Olsen*, 2004]. Alternatively they can develop from gravity instabilities, commonly in the internal parts of cordilleran and collisional orogens, related with late- or post-orogenic extensional processes, such as arching of detachment faults due to isostatic rebound [core complexes; *Coney and Harms*, 1984; *Lister and Davis*, 1989], or flow of partially molten rocks [*e.g. Whitney et al*., 2004, *Vanderhaeghe*, 2004]. Only the latter represent the original concept of *Eskola* [1949].

Some gneiss domes exhibit magnetic anomalies, e.g., the Baltimore gneiss domes, where this characteristic was used to identify one of them [*Higgins et al*., 1973]. Positive magnetic anomalies characterize many other Appalachian domes, such as those of the Bronson Hill Anticlinorium in New England, and domes and basement outcrops in Massachusetts, Connecticut, New Jersey and SE New York [*Harwood and Zietz*, 1974; *Zietz et al*., 1980]. The cause of these anomalies has been ascribed to the existence of magnetic rocks in the basement, so they may not necessarily result from the doming process. The same accounts for the Baltimore gneiss domes, where the anomalies are magnetic lows, which could be explained by remanent magnetization from a geological period of reverse polarity of the Earth's magnetic field. However, *Harwood and Zietz* [1974] report that in the Berkshire Highland, straddling between Connecticut and New York, magnetite is abundant in local gneiss units that underwent the higher grades of Paleozoic metamorphism. They suggest that metamorphism could explain the different magnetic patterns found on the Precambrian basement.

Magnetic anomalies also occur in gneiss domes in the Variscan belt, such as the Saxon Granulite Massif and the Erzgebirge, in the Bohemian Massif [*Gabriel et al*., 2011]. These are late orogenic domes, and their magnetic components may be inherited from the Saxothuringian continental basement. However, it is also possible that they developed metamorphic ferromagnetic minerals during the Variscan orogeny, when they were subducted and then exhumed by an extensional detachment or as a hot, low-viscosity intrusion [*Franke and Stein*, 2000 and references therein].

A case for magnetization related with extensional collapse and doming was made for the Eastern Galicia Magnetic Anomaly (EGMA) in the late Variscan Lugo and Sanabria domes by *Ayarza and Martínez Catalán* [2007]. This anomaly was defined by *Aller et al.* [1994], and is a salient feature of the aeromagnetic map of the Iberian Peninsula, as shown in Figure 1. It is a roughly N-S band, 190 km long and 50 km wide, slightly concave to the E, with maximum amplitude of 190 nT.

This paper aims to improve our understanding of the EGMA. New ground-based magnetic data have been acquired in and around the Xistral Tectonic Window of the Lugo Dome, improving the resolution of the previous aeromagnetic map. Based on the new map, on additional measurements of magnetic susceptibilities of rocks and on a good knowledge of the

geology of the area, several cross sections have been modeled to link the anomalies with their sources and the Variscan evolution.

2. Geological Setting

The geology of NW Iberia includes an autochthonous domain, a parauchthonous thrust sheet a few kilometers thick, and an allochthonous nappe stack. A cross section along the northern Spanish coast (Figure 2a) depicts these domains together with the main structures, and an interpretation of the present continuation of the main crustal-scale contractional shear zones deep in the crust. The latter is largely based on four reflection seismic profiles (Figure 2b), two of them acquired on land, ESCIN-1.1 and 1.2, and two offshore, parallel to the coast, ESCIN-3.2 and 3.3 [*Pérez-Estaún et al*., 1994, 1995; *Álvarez-Marrón et al*., 1995, 1996; *Martínez Catalán et al*., 1995; *Ayarza et al*., 1998, 2004]. Their location is shown in Figure 1a.

The Autochthon is formed by metasediments, metavolcanics and orthogneisses respectively deposited, extruded and intruded during the Neoproterozoic and Paleozoic in the northern Gondwana margin, as indicated by sedimentary and faunal evidence and by detrital zircon age populations [*Robardet*, 2003; *Martínez Catalán et al*., 2004; *Shaw et al., 2014*; *Gutiérrez-Alonso et al*., 2015].

The Parautochthon consists of Cambrian, Ordovician and Silurian metasediments and volcanics exhibiting stratigraphic and igneous affinities with the Autochthon, and representing a distal part of the Gondwanan continental margin [*Farias et al*., 1987; *Dias da Silva et al*., 2014a]. Deformation and metamorphism are Variscan, and early Carboniferous syn-orogenic flysch-type deposits related with the emplacement of the allochthonous complexes occur in both the Autochthon and Parauthochthon, [*Martínez Catalán et al*., 2008; 2016; *Dias da Silva et al*., 2014b].

The Allochthon is formed by units characterized by a unique lithologic association and tectonometamorphic evolution. They are grouped by their lithologic affinities and their relative position in the nappe pile, and appear separated from each other by thrusts or extensional detachments. These units include pieces of the outermost basement of Gondwana, ophiolites derived from a Paleozoic oceanic realm, and fragments of an ensialic Cambro-Ordovician island arc [*Arenas et al*., 2007; *Martínez Catalán et al*., 2007; *Sánchez Martínez et al*., 2007].

Figure 3 illustrates the main structural features of the three domains in northern Galicia (NW Spain). The aeromagnetic and Bouguer gravity anomalies of the same region are shown in Figure 4.The Cabo Ortegal, Órdenes and Malpica-Tui allochthonous complexes appear in the western half of the map, together with the Parautochthon, and include allochthonous units belonging to three different groups. Many of these units registered early Variscan high pressure metamorphism related with subduction during the closure of the ocean [*Martínez Catalán et al*., 2009, and references therein]. This was followed by a Variscan collisional evolution in common with that of the Parautochthon and Autochthon, and which includes contractional (C) and extensional (E) events. The Autochthon is represented in the map by the West Asturian-Leonese Zone (WALZ), which occupies its eastern half, and the Ollo de Sapo Domain of the Central Iberian Zone (CIZ), a narrow, curved strip in the center. The name of the latter derives from the Ollo de Sapo (toad's eye) Fm., a Lower Ordovician ensemble of porphyritic felsic volcanic, volcaniclastic and subvolcanic rocks with bluish quartz and large K-feldspar phenocrysts [*Parga Pondal et al*., 1964; *Díez Montes et al*., 2010].

The three allochthons where assembled in an accretionary prism during early Variscan plate convergence, (Middle and Upper Devonian), related with oceanic closure and subduction [*Martínez Catalán et al*., 2009; *Arenas et al*., 2016]. At the beginning of the Carboniferous, a collisional regime was installed, and several contractional episodes have been distinguished [*Martínez Catalán et al*., 2014; *Alcock et al*., 2015]. C1 produced recumbent folds with E vergence in the three tectonic domains. It was followed by thrusting of the Allochthon above the Parautochthon, and by the emplacement of the whole pile above the Autochthon of the CIZ. Then, thrusting and imbrication continued in the WALZ and the Cantabrian Zone (CZ). This episode is described as C2, and as C1, it was diachronous, progressing toward the E, that is, toward the foreland. In the hinterland, C1 and C2 occurred during the Lower and Middle Mississippian, but in the CZ, a typical foreland thrust belt, imbrication was active until the end of Carboniferous [*Pérez-Estaún et al*., 1988].

Major contractional Variscan structures are depicted in Figure 2a, which includes a sketch of the evolution of the different deformation episodes along the section in relation with their ages. The figure is based on data by *Pérez-Estaún et al*. [1988], *Dallmeyer et al*. [1997], *Martínez Catalán et al*. [2003, 2014] and *Alcock et al*. [2015]. Large recumbent folds are especially well developed in the Mondoñedo Nappe (Figure 3, Section 1), whereas several large thrust faults occur in the Allochthon and the Parautocthon [*Martínez Catalán et al*., 2002]. The Mondoñedo Nappe, originally defined as a large recumbent fold by *Matte* [1968], is bounded by a basal thrust fault [*Bastida et al*., 1986; *Aller and Bastida*, 1993] which was partially reactivated later as an extensional detachment.

Gravitational collapse followed the main phases of compression and crustal thickening after 10-20 m.y. of thermal relaxation [*Alcock et al*., 2009, 2015]. Low-dipping extensional detachments played the main role in crustal thinning, but also domes triggered by heating gave rise to collapse and extension. The extensional process was active during the whole Pennsylvanian in the internal zones. However, it was interrupted by upright folding associated with strike-slip, ductile shear zones, such as the left-lateral Palas de Rei and a right-lateral shear zone to the W of the Malpica-Tui Complex (Figure 3). Tight, upright folds characterize the Ollo de Sapo Antiform and the Malpica-Tui and Cabo Ortegal synforms. These structures are ascribed to event C3, and consequently, we differentiate two extensional events, E1 and E2, pre- and postdating C3 respectively.

Domes and detachments are clearly related. Some detachments were formed in the limbs of domes, but also, E2 domes frequently overprinted previous (E1) extensional detachments and in some cases developed their own new detachments, as is the case of the Viveiro shear zone and fault in the Lugo Dome. E1 domes are recognized because they were affected by later upright folds, while others developed after C3. Late Variscan migmatites and inhomogeneous granitoids, partly derived *in situ* by partial melting of high-grade paragneisses, are abundant in the domes, and were intruded by younger but still Variscan homogeneous leucogranites. All these features characterize gneiss domes [*Whitney et al*., 2004], which result from regional-scale crustal flow with the addition of magmas of crustal density [*Block and Royden*, 1990; *Thompson and McCarthy*, 1990]. Structural and metamorphic descriptions of the main Galician detachments can be found in *Martínez Catalán et al*. [1996, 2003], *Díaz García et al*. [1999], *Arenas and Martínez Catalán* [2003], *Gómez Barreiro et al*. [2010] and *Díez Fernández et al*. [2012].

The large domes alternate with large synforms and structural basins where low-grade metasedimentary rocks occur. The allochthonous complexes are preserved as klippen in some of these synforms, usually lying above low- to medium grade metasedimentary rocks of the Parautochthon.

The largest synform is occupied by the Órdenes Complex, whose structure is shown in the geological sketch of Figure 3, Section 2. A detailed magnetic map of this complex was acquired on land, and an interpretation of the gravimetric and magnetic anomalies was made by *Martínez Catalán et al.* [2012]. There, the sources of magnetic anomalies are serpentinized ultrabasic rocks, and in some cases basic rocks, occurring in units bounded by thrust and detachment faults.

The EGMA coincides with two late Variscan structural, metamorphic and locally anatectic domes. The Lugo Dome [*Capdevila*, 1969], to the N, occurs in the WALZ at the limit with the adjacent CIZ, while the Sanabria Dome, to the S, is entirely inside the CIZ, in the Ollo de Sapo Domain (Figure 1). At the northern part of the Lugo Dome, the Xistral Tectonic Window exposes deep parts of the middle crust, revealing the tectonometamorphic history of late Variscan extension [*Martínez Catalán et al*., 2003; *Arenas and Martínez Catalán*, 2003; *Alcock et al*., 2009].

The basal thrust of the Mondoñedo Nappe was partially reactivated as a detachment downthrown to the E, and several other detachments developed at its relative autochthon (Figures 3 and 5), the main of which is the Lower Extensional Detachment. It underlies the Xistral Quartzite, formed almost exclusively of quartz and whose resistance to weathering and erosion has formed the Sierra do Xistral. This quartzitic unit reached locally a structural thickness of *c.* 5000 m after folding (Section 1 in Figure 3). The Lower Extensional Detachment overprints previous recumbent folds and thrust faults, and is actually the upper boundary of a ductile shear zone where intense shearing affects underlying schists, quartzites and paragneisses. These rocks crop out between Viveiró and Xove (Figure 5), at the core of an open antiform where abundant migmatites and inhomogeneous granites are also found. It is the same fold that defines de Lugo Dome and controls the geometry of the Xistral Tectonic Window. Kinematic criteria indicate a top to the E sense of motion of the detachment, and a subtractive metamorphic offset indicates that this is an extensional structure [*Arenas and Martínez Catalán*, 2003; *Martínez Catalán et al.*, 2003].

The Lugo Dome folded the Mondoñedo thrust sheet, whose relative autochthon crops out at the tectonic window (Figure 5), and also the reactivated basal shear zone and other extensional detachments. However, the Viveiro Fault was coeval with the rise of the dome, and represents the latest extensional detachment in the region.

Early Variscan granitoids in the northern part of the Lugo Dome have yielded U-Pb zircon and monazite ages of 315 ± 2 Ma for the Viveiro granodiorite, a synkinematic intrusion cropping out between Viveiro and Vilachá, and *c.* 317 ± 7 Ma for the Penedo Gordo granite, between Ourol and Viveiro (Figure 5). The latter is deformed in the shear zone associated to the Viveiro Fault. The youngest massifs include A Tojiza granodiorite, a rounded pluton cropping out between Ferreira and Mondoñedo, dated at 295 ± 2 Ma, and the San Cibrao leucogranite, dated at 286 ± 2 Ma [*Fernández-Suárez et al*., 2000]. The inhomogeneous granites and the late Variscan leucogranites are commonly weathered, and given the outcropping conditions, these two lithologies are difficult to discern, and are mapped together in Figure 5.

Slates, schists and granites of the Mondoñedo thrust sheet in and around the Lugo Dome yielded $^{40}Ar/^{39}Ar$ ages between 298 and 274 Ma [*Dallmeyer et al*., 1997]. These data imply that high temperatures in the dome lasted from before 315 to 275 Ma. On the other hand, the geometry of the dome is asymmetrical, marked by the development of a late extensional detachment to the W, the Viveiro Fault. Comparing with thermomechanical models of *Tirel et al*. [2004] both, ages and geometry indicate a slowly developing dome that has reached its mature stage.

3. Geophysical Framework

3.1. Magnetometry

The first interpretation of the magnetic anomaly occurring at the western of the Lugo Dome was made by *Aller* [1986] using the residual anomaly extracted from the isolines of the total magnetic field of Spain [*Instituto Geográfico Nacional*, 1975], a low-resolution map based on ground measurements. He also used an aeromagnetic map of eastern Galicia and NW of the León province provided by the Compañía General de Geofísica S.A. *Aller* [1986] modeled the anomaly using a block with a flat upper surface at a depth of 5 km, and a contrast of magnetic susceptibility of 0.0126 SI in relation with the country rocks. Geologically, he interpreted the anomaly as due to a series of igneous intrusives of intermediate or basic composition.

After the publication of the aeromagnetic map of the Spanish part of the Iberian Peninsula [*Instituto Geográfico Nacional*, 1987; *Ardizone et al*., 1989], *Aller et al*. [1994] named this feature as it is known today, the Eastern Galicia Magnetic Anomaly (EGMA). The authors made 2.5D models of five sections using magnetic susceptibilities κ = 0.045-0.055 SI for the most magnetic blocks, and suggested that the source could be basic and ultrabasic rocks imbricated in the middle crust by the Mondoñedo Nappe basal thrust and by an underlying eastern Galicia thrust. Other possible sources envisaged by *Aller et al*. [1994] were peridotites, pyroxenites and hornblendites, locally serpentinized, cropping out in the vicinity of the Viveiro Fault, in association with Variscan synkinematic calc-alkaline granodiorites [*Galán*, 1987]. However, these rocks do appear only in just a few small spots, and never at the Viveiro Fault. Moreover, their relationship with the synkinematic granodiorites was put into question by the age of 293 ± 3 Ma obtained in the hornblendites by *Fernández-Suárez et al.* [2000], at odds with the 317 ± 7 Ma calculated for the granodiorites by the same authors.

Ayarza and Martínez Catalán [2007] made a different interpretation of the EGMA based on the aeromagnetic map of *Ardizone et al*. [1989]. They also relied on *in situ* measurements of the magnetic susceptibility of outcropping rocks, and on realistic, newer geological grounds which disregarded the staircase geometry assumed for the Mondoñedo Nappe basal thrust by *Aller et al*. [1994]. Alternatively, the extensional tectonics overprinting thrust tectonics was given a prior role, and an extensional origin was proposed for the dome and the anomaly. *In situ* measurements were critical, as it was found that rocks cropping out abundantly at the core of the Xistral Tectonic Window –paragneisses, migmatites and inhomogeneous granites– often had high susceptibilities.

The authors found that multi-domain magnetite was the main carrier of induced magnetization, reaching sizes visible to the naked eye in migmatites (Figure 6) and inhomogeneous granites. It occurs as equigranular, often idiomorphic individual grains up to 1 cm in diameter. Petrographic analysis using reflected light shows exolved ilmenite in magnetite grains, as well as replacement of the latter by hematite [*Ayarza and Martínez Catalán,* 2007]. Elongated magnetite grains were found in well-foliated paragneisses, also partially replaced by other Ti-Fe oxides. Small massifs of basic and ultrabasic rocks inside the migmatites and high-susceptibility iron ore bodies sparsely distributed in low-grade Middle Ordovician slates were found to contribute to the anomaly only to a minor extent.

Consequently, 2D-2.75D models were built for four sections along the Lugo Dome using a large, lens-shaped body of migmatites, up to 12 km thick and 80-130 km wide, with κ = 0.030 SI. Models with the large lens of migmatites with κ = 0.020 SI, plus a magnetic lower crust with κ = 0.025 SI, were considered equally valid, except for depths below the Curie

temperature for magnetite (575 ºC). This interpretation ruled out the need of basic/ultrabasic rocks as magnetic sources, since they are really scarce at surface and probably also at moderate depths, according to the Bouguer gravity anomaly (Figure 4b).

The EGMA has been also related with magnetic anomalies at the South Armorican continental shelf, based on their continuity on each side of the Bay of Biscay, and their similar wavelengths and intensities [*de Poulpiquet,* 2012]. According to this author, the magnetic arc defined by these anomalies fits the geometry of the Ibero-Armorican Arc. Thus, he interpreted the anomaly as the result of an aborted Cambro-Ordovician rift which created a narrow oceanic basin in the present Armorican continental platform, and a sedimentary trough, perhaps an aulacogen, in NW Iberia.

In his contribution, *de Poulpiquet* [2012] pointed out that in the Armorican continental plateau, the magnetic anomaly is accompanied by a positive gravity anomaly, which is absent in the EGMA. He describes a positive, long wavelength (80 km) gravity anomaly in the central part of the EGMA, between the Lugo and Sanabria domes, which he interprets as resulting from a deep, dense source between 12.5 and 23 km, similar to that of *Aller et al.* [*1994*]. His model also includes an upper source, 4.5-11 km deep, corresponding to the low density magnetic migmatites of *Ayarza and Martínez Catalán* [2007]. However, its gravity maximum is displaced 10 km to the SW with respect to the magnetic maximum, and coincides with the Middle Ordovician slates of the Ollo de Sapo Domain, whereas the magnetic maximum lies above the Viveiro Fault.

Regardless of its relationship with the South Armorican anomalies, the EGMA is not an isolated feature. In the Iberian Massif, it represents the northern branch of a much larger anomaly that can be continued until central Spain and then to the W and NW in central and northern Portugal, forming the inner region of an arc defined by anomalies of lesser wavelength and amplitude (Figure 1b). This arc is also delineated by early Variscan folds and has been historically called Castillian bend [*Staub*, 1926, 1928], Oretain-Iberian Arc [*Llopis Lladó*, 1966], and Central Iberian Arc [*Martínez Catalán*, 2012], while *Aerden* [2004] considered it as part of an S-shaped Ibero-Armorican orocline.

3.2. Gravimetry

The Bouguer gravity anomaly map of the Iberian Peninsula and the Balearic Islands was published by the *Instituto Geográfico Nacional* [1996; see also *Mezcua et al*., 1996]. Two years later, 973 new gravity measurements were made in Galicia in the framework of a project led by the Spanish Agency of Nuclear Wastes (ENRESA), and merged with the pre-existing data. A new Bouguer anomaly was recalculated for the entire new dataset using the Geodetic Reference System formula of 1967 (GRS-67) and a mean density of 2670 kg/m^3.

Figure 4b shows the Bouguer gravity anomaly in northern Galicia and Figure 4c shows its vertical derivative. The intensity of the latter is proportional to that of the magnetic anomaly reduced to the pole when the source of gravity and magnetism coincides. However, the existence of magnetic remanence disturbs the distribution of magnetic maxima and minima, and integration of both datasets should be treated with caution. Figure 4 allows us to further analyze if the source of the EGMA might correspond to dense basic rocks. The largest elongated maxima of the Bouguer's vertical derivative surrounding the Lugo Dome reflect the outcrop of dense rocks, the Ordovician and Cambrian slates W of the Viveiro Fault and at the Bretoña Synform, to the E of the dome (Section 1 in Figure 3). Conversely, the magnetic anomaly is caused by lighter rocks, and its maxima occur between the two elongated maxima

of the gravity vertical gradient, coinciding with the central and western parts of the Lugo Dome.

A gravity model for Section 1 (Figures 3 and 4b), built with GM-SYS, Geosoft Inc., is shown in Figure 7. It cuts across the Cabo Ortegal Complex, the Ollo de Sapo Antiform, the Lugo Dome and the Mondoñedo thrust sheet. The densities are similar to those used in previous models by *Ayarza and Martínez Catalán* [2007] and *Martínez Catalán et al*. [2012], and are mean values –rounded to multiples of 10– of samples collected in the different domains and measured in the laboratory, with the exception of those for the lower crust and mantle. The value for migmatites (2650 kg m^{-3}) has been lowered somewhat to adapt the calculated anomaly to the rather well constrained geology. The density for the Upper Allochthon of the Cabo Ortegal Complex (2860 kg m^{-3}) is a weighted average between that of basic rocks (3000-3500 kg m^{-3}), and paragneisses (2700 kg m^{-3}), except in the basal lens (2870 kg m^{-3}), where amphibolites dominate. The ophiolites at the western side of Cabo Ortegal Complex and those to the W, which belong to the adjacent Órdenes Complex, have been modeled with the same density (2870 kg m^{-3}). High densities (2790 kg m^{-3}) characterize non-weathered Cambrian and Ordovician slates corresponding to the low-temperature zone of the greenschist facies. But density decreases when higher temperatures were reached, and 2640-2680 kg m^{-3} were typically measured in schists. The final values used in the model are shown in Table 1 and depicted in Figure 7.

The Bouguer anomaly, which shows an irregular but generalized decrease to the SE, is modeled with a step at Moho level, roughly beneath the Viveiro Fault or the Ollo de Sapo Antiform (Figures 2 and 7). This geometry is based on the image provided by seismic reflection profiles shown in Figure 2b [*Álvarez-Marrón et al*., 1966; *Martínez Catalán et al*., 1995*; Ayarza et al*., 1998, 2004]. The Moho discontinuity is assumed to occur at the base of a highly reflective band representing the lower crust. Its thickness varies from 8-12 s two-way travel time (TWTT) in profile ESCIN-1.1, to 9-12 s in profile ESCIN-1.2, to 7-12 s in most of profile ESCIN-3.3, and to 8-10 s at its westernmost edge and in profile ESCIN-3.2. The Moho step separates the more internal, seismically transparent and thinner crust under the GTMZ and CIZ from a thicker reflective crust to the E, beneath the WALZ and CZ.

The 7-12 s reflections of profile ESCIN-3.3, actually consists of two reflective bands suggesting a duplication of the lower crust. *Ayarza et al*. [1998] interpreted this feature as due to the important shortening (> 50%) underwent by the CZ, a thin-skinned thrust belt 180 km wide [*Pérez-Estaún et al*., 1994; *Martínez Catalán et al*., 2003]. As its basement was not involved in the upper crustal imbrications, some 100 km of it could have underthrusted the WALZ to the W late in Variscan times, [*Ayarza et al*., 1998, 2004], its edge forming the Moho step seen in profile ESCIN-3.3 [*Martínez Catalán et al*., 2003, 2014].

The same authors suggested the possibility that the duplication were due to the Alpine convergence, based on another seismic profile oriented N-S acquired in the SE of the CZ, and where a crustal imbrication is seen [*Pulgar et al*., 1996]. This is not however our preferred option because the base of the crust occurs there at 12 s TWTT far from the Alpine imbrication, and reaches more than 15 s when imbricated. We assume that 12 s represent the typical crustal thickness of the CZ and WALZ, because profile ESCIN-1.2 images the CZ/WALZ transition, and a highly reflective lower crust reaching 12 s straddles both zones.

Underthrusting of the CZ basement does not represent a mechanical. Extension in the CIZ and the western part of the WALZ developed following severe crustal thickening mostly due to the emplacement of the Allochthon at *c*. 345-340 Ma (Figure 2a). Thrusting continued until *c*. 325 Ma in the WALZ and until 295 Ma in the CZ, but crustal thickening was moderate because only the sedimentary cover became involved [*Pérez-Estaún et al*., 1988, 1994;

Dallmeyer et al., 1997; *Martínez Catalán et al*., 2003, 2009, 2014; *Alcock et al.,* 2015]. The extensional detachments and domes developed at *c.* 330-295 Ma. This implies that while the crust of the CIZ and western WALZ was being re-equilibrated, that of the CZ remained cold while being deformed by thin-skinned tectonics. The more external parts of the CZ were strongly shortened by imbrication at the very end of the Carboniferous, around 300 Ma, and its cold basement was then underthrusted beneath the relatively thin central and eastern parts of the WALZ and its already re-equilibrated and thin western part.

In the gravity model, the crust W from the Moho step is 27 km thick, while to the E, it reaches 35 km (Figure 7). The step would then represent a preserved root of the Cantabrian Zone, while the crustal-scale shear zones that probably existed separating the roots of the other significant domains (Navia and Alto Sil, Mondoñedo Nappe and Parautochthon) are no longer preserved due to re-equilibration (dotted lines in Figure 2a).

In addition, the model shows that the gravity minimum in the middle of the profile (Figure 7) responds to the low density massive Xistral Quartzite and the migmatites cropping out in the tectonic window. However, these low densities are not enough to fit the anomaly. Accordingly, differences in crustal thickness are needed to explain the low gravity values. This option is supported by the results of deep seismic reflection profiling, while the alternative hypothesis of significant increase in crustal density to the W lacks of any independent support and opposes estimated densities of outcropping geology. Thus, dense rocks are not necessary to fit the Bouguer anomaly in the EGMA area.

4. Magnetic Anomaly of the Xistral Tectonic Window

Previous interpretations of the Magnetic Anomaly of the Lugo-Sanabria Dome, some of them crossing the Xistral Tectonic Window, are based on the aeromagnetic map of Spain of *Ardizone et al*. [1989] or even on older sources [*Aller*, 1986]. Being important to the regional scale, the aeromagnetic map of Spain has a limited resolution, as it was flown at 3000 m above sea level, and along N-S lines separated 10 km with E-W control lines every 40 km. The acquisition lines are drawn in Figure II.2 of *Ardizone García* [1998], and are shown in Figure 4a, which shows the northern half of the EGMA. The whole EGMA was sampled by 12 N-S and 8 E-W lines, while the Xistral Tectonic Window was sampled just by barely 5 N-S and 2 E-W flight lines (Figure 4a). Even if the nominal separation between measurements along the lines was 34 m, the line interval is too large to image the shorter wavelength anomalies related to outcropping lithologies and structures such as those shown in Figure 5. To obtain a higher resolution magnetic map, new ground data have been acquired covering the whole tectonic window and its surroundings.

4.1. Data Acquisition and Processing

Two Geometrics G-856 proton magnetometers with a resolution of 0.1 nT were used in the acquisition. One of them registered the Earth's magnetic field in a base station every 5 minutes in order to control the diurnal variation. A preliminary land survey was made in this area in September, 2009, but most data were acquired in two campaigns in April, 2015 and May, 2016. Both seasons coincided with a period of rather stable solar activity, which was checked every day in NOAA's space weather scale (http://www.swpc.noaa.gov/SWN/). The reference base station was established 3 km S of Viveiro (UTM: E613923, N4832265; height: 141 m), in the NW of the Xistral Tectonic Window. Measurements were taken as far as possible from power lines, buildings, cars and other metallic objects, and looking for the best

signal intensity and coherence of measured magnetic field intensity in places with strong magnetic gradients.

The survey covered an area of *c.* 750 km^2, with 315 measured stations, implying a density of 0.42 data km^{-2}. Diurnal and secular variations were corrected, and absolute anomalies were calculated with respect to the International Geomagnetic Reference Field (IGRF) using the package Oasis montaj of Geosoft Inc. All data were referred to April 14th, 2015, for which, the IGRF at the base station was 45861 nT, with an inclination of 58.72º N and a declination of 2.537º W (Table 1). Data acquired during this survey are provided in Table S1 of Supporting information.

The highest and lowest values of the absolute anomaly were 777 and -437 nT. All values were recalculated and plotted in a grid of 250 m for which maximum and minimum are respectively 737 and -403 nT. Despiking was not considered necessary given the smooth distribution of absolute values, and the fact that gridding eliminated the extreme values. The absolute anomaly map is shown in Figure 8a, where faults and contacts have been included to allow comparison with the geological map of Figure 5. A map of the absolute anomaly reduced to the pole (RTP) is depicted in Figure 8b, aiming to place each anomaly above its source.

Figure 8c shows a map of geological domains and dominant lithologies, together with values of the magnetic susceptibility (κ) measured with a portable susceptometer Kappameter KT-6. Each datum represents the mean of several measurements in an outcrop, and only locations where $\kappa \geq 0.001$ SI are shown. These measurements, together with their coordinates, are provided in Table S2 of Supporting information. Figure 8d shows the vertical derivative of the Bouguer anomaly for the study area. An upward continuation of the measured magnetic anomaly to 3000 m above sea level is shown in Figure 9a, to allow comparison with the aeromagnetic map flown at the same height (Figure 9b).

Some lenses of amphibolites, up to 3 km long, had been mapped in the southern part of the tectonic window (Figure 5). They are pre-Variscan basic and ultrabasic intercalations in the Xistral Quartzite, probably sills [*Capdevila*, 1966]. In one of the lenses, a high susceptibility, up to 0.1 SI was measured, but κ was very low in the lenses cut across by Section D (Figure 4). For that reason, and also because of their relatively small volume, these rocks have not been further considered in the models.

Rocks with high magnetic susceptibility also exist outside the Xistral Tectonic Window, in the Middle Ordovician Luarca Slates of the Ollo de Sapo Domain, to the W and NNW of Viveiro. Sedimentary deposits of ooidal iron oxides are common in the Luarca Slates, but there, a 2 to 20 m thick layer was locally transformed in ironstone rich in magnetite by contact metamorphism induced by the intrusion of a Variscan granitoids [*Lunar Hernández*, 1977]. The ironstone was worked between 1896 and 1966 in A Silvarosa and Galdo mines, W and SW from Viveiro [*Gutiérrez-Marco and Rábano*, 2014], and susceptibilities up to 0.2 and 0.4 SI were measured in some outcrops (Figure 8c). But the contribution to the regional anomaly is unnoticeable in the aeromagnetic map (Figure 9b), and minimum in the ground-based map (Figure 8a).

In addition to ground-based measurements of the Earth´s magnetic field and *in situ* sampling of the magnetic susceptibility, oriented samples were drilled in outcrops of the Xistral Tectonic Window. The rocks sampled include Cambrian schists and quartzites inside the shear zones under the Lower Extensional Detachment and the Viveiro Fault, the underlying paragneisses and migmatites corresponding to the Neoproterozoic Vilalba Series, and

inhomogeneous granites that represent advanced stages of migmatization involving large amounts of partial melting.

The drilled cores have been analyzed for anisotropy of magnetic susceptibility (AMS) and remanent magnetization using alternate fields and thermal demagnetization. Magnetic mineralogy was identified by their thermomagnetic curves and using a Variable Field Translation Balance (MMVFTB, Laboratory of Paleomagnetism, University of Burgos). The results, involving more ongoing analyses, will be presented in another contribution aimed to interpret magnetic remanence and processes leading to magnetization. Some of the data necessary for the interpretation of the anomalies in terms of the macrostructure are advanced here.

4.2. Structural Interpretation of the Ground-based Magnetic Anomaly

Four sections across the magnetic anomaly shown in Figure 8a were modeled in 2D using GM-SYS. The sections were chosen across the Xistral Tectonic Window and cutting representative structures, mainly extensional detachments (Figure 5), at places where they coincide with maxima and minima of the magnetic anomaly. The RTP version of the anomaly (Figure 8b) shows a coincidence between several highs and the extensional detachments, with most important maxima occurring along the Viveiro Fault. For modeling purposes, we have used an upward continuation to 200 m to smooth the short-wavelength anomalies caused by highly magnetic outcropping rocks without modifying them substantially.

4.2.1. Models Using Magnetic Susceptibility

Figure 10 shows the results of modeling assuming that magnetization is entirely induced by the present Earth magnetic field, thus using the magnetic susceptibility as the only source of the anomaly. Geological cross sections in the background, including the faults and the different units, are depicted using the same colors as in Figure 5. A preliminary version of these sections was used as a backdrop to correctly place the model blocks in relation with the structures. This version was later slightly modified in depth to fit the structures to the model blocks, and the sections shown in Figure 10 result from this adjustment.

The calculated magnetic anomaly (thin black line) has been approached using the observed values of the absolute anomaly, shown by black dots. The thick grey line shows the RTP anomaly, for comparison with the outcrop of detachments. Magnetic blocks are depicted bounded by a red line, with the value of magnetic susceptibility indicated. Outside these blocks, susceptibility is assumed to be zero.

Models are limited to a depth of 5 km because the effect of the rocks underneath is negligible on the ground-based anomaly. Only in Section D blocks have been continued laterally down to 6 and 8 km to adjust both ends of the anomaly. 2D modeling is used due to the along-strike continuity of the structures (Figure 5), and because it was observed that limiting the blocks to ± 10 km in the direction of structures (nearly perpendicular to the sections) had no a significant effect on the calculated anomaly.

The Bouguer anomaly is included in Figure 10 but was not modeled, except for Section C, a part of geological Section 1 of Figure 3 for which the gravity model is shown in Figure 7. In all four sections, the gravity anomaly shows a relatively steep drop above the tectonic window, which is mainly related with the step at the Moho level that characterizes the thicker crust in the E shown in Figure 7, but also with lithologies E and W of the Viveiro Fault.

In situ measurements of magnetic susceptibility show an extreme variability (Figure 8c), suggesting a rather inhomogeneous original distribution of magnetite, although differences in weathering may also play an important role. High susceptibilities are only found in the Middle Ordovician ironstones to the W of the Viveiro Fault, and in quartzites, paragneisses, migmatites and inhomogeneous granites inside the tectonic window. Cores were drilled in 39 sites in the tectonic window at places where field susceptibility values were higher than 0.001 SI. Detailed values of those samples were later measured with a susceptometer Kappabridge KLY 45 in the Laboratory of Paleomagnetism of the University of Burgos. For each site, 2 to 12 cores were used and a mean value was calculated. The mean of all these samples is κ = 0.0099 SI (see Table 1 for a list of numerical values).

Given the inhomogeneous distribution of magnetization, we have tried to build the models as simple as possible using integer multiples of κ = 0.01 SI for the blocks, except for A Tojiza granodiorite in Section C, whose susceptibility measured *in situ* is around 0.001 SI. The magnetic field used in all models is the mean value of the IGRF calculated for all the stations at April 14th, 2015: B = 45817.6 nT, I = 58.6º, D = -2.5º.

As shown in Figure 10, the magnetic anomalies have a relatively short wavelength, about 10-12 km, and locally 3 km in Section C. Variability is related with the spacing of sampling and that of the main extensional structures, which had been identified previously [*Martínez Catalán et al*., 2003]. Wavelengths in the newly acquired data are always lesser that the *c*. 28 km shown by the EGMA in the aeromagnetic flight (Figures 4a and 9b). Even the upward continuation to 3000 m of the ground anomaly (Figure 9a) lacks the smooth appearance of the aeromagnetic dataset due to its higher resolution.

Next, we include a description of the models explaining how the blocks of Figure 10 have been designed and why:

- The Middle Ordovician, magnetite-rich ironstone has been modeled as a rather thin folded bed in Section A, as it may be responsible for the first, weak maximum to the WNW. Two different susceptibilities have been used, 0.04 for the uppermost part, and 0.08 for the rest. Although values up to 0.4 SI were measured in localized outcrops, our values fit the anomaly in combination with the thickness used. Thinner blocks combined with higher susceptibilities would equally match the measured anomaly.

- The Neoproterozoic Vilalba Series show different degrees of migmatization, often transformed into inhomogeneous granites and variably intruded by late Variscan leucogranites. The ensemble has been modeled in all sections as a 1-4 km thick band with a magnetic susceptibility κ = 0.02 SI. The block is folded by the Lugo Dome and crops out at its core in Sections A and B. The κ value chosen is higher than most measured values, but this is a common problem encountered in all lithologies of the Xistral tectonic window, and is attributed to weathering close to the surface and to heterogenities. This block can be interpreted as a downward continuation of the shear zone below the Lower Extensional Detachment. Its thickness is not constrained, and could be increased without significantly changing the calculated anomaly.

- The lowermost part of the Cambrian crops out beneath the Lower Extensional Detachment, and their metasedimentary rocks are often characterized by high magnetic susceptibilities. They include schists, paragneisses and quartzites of the Cándana Group that were deformed in the shear zone beneath the detachment and the Xistral Quartzite, which occupies its hanging wall. It is worth noting that the same rocks from the Mondoñedo thrust sheet do not exhibit magnetic properties, except at its reactivated basal shear zone. The shear zone has been modeled with blocks 0.5-2 km thick folded by the

Lugo Dome, with $\kappa = 0.04$ SI. Two lenses with $\kappa = 0.06$ SI have been added in Section C to match the observed anomaly.

- Another extensional structure, interpreted as joining the Lower Extensional Detachment toward the SE, was mapped in the Xistral Quartzite to the SW of Rúa, and supposedly continues in the inhomogeneous granites to the NE (Figure 5). The inhomogeneous granites, like the migmatites, are frequently magnetic, while the late Variscan leucogranites are not, although both lithologies are undifferentiated in Figure 5. This detachment coincides with a local maximum in Sections A and B, and has been modeled with small blocks of limited, variable thickness and $\kappa = 0.02$ and 0.04 SI.

- The Mondoñedo Nappe Basal Thrust was overprinted or reactivated by an extensional shear zone, folded by the Lugo Dome and whose large SE limb dips 15-25º SE [*Martínez Catalán et al*., 2014]. This extensional structure affects Cambrian schists and quartzites with high magnetic susceptibilities, and has been modeled as a thin block with $\kappa = 0.02$ or 0.04 SI.

- The Viveiro Fault was the latest extensional structure, and its associated shear zone seems to be the main contributor to the EGMA. High magnetic susceptibilities have been measured even in the Xistral Quartzite, which is non-magnetic in the rest of the tectonic window, probably because it occurs at the hanging wall of the Lower Extensional Detachment, and so, it was only weakly affected at its base by the shear zone. However, when sheared by the Viveiro Fault, magnetite grew even in these nearly pure quartzites. The shear zone has been modeled with blocks dipping 15º-25º NW, 1-3 km thick, and with $\kappa = 0.06$ and 0.08 SI. Thickness and susceptibility were increased in the southern sections to fit the observed high anomaly values. The Viveiro shear zone overprints the one under the Lower Extensional Detachment, whose blocks had been thinned or suppressed in all models but Section D.

4.2.2. Models Including Magnetic Remanence

Remanent magnetization (M_r) was measured in 39 samples in the Laboratory of Paleomagnetism of the University of Burgos with a 2G-755 cryogenic magnetometer, using 2 to 12 cores for each site. The magnetic susceptibility (κ) had been previously measured, and the induced magnetization (M_i) was calculated using a magnetic field of 36.1186 A m^{-1}. Then, the Königsberger ratio ($Q_n = M_r/M_i$) was obtained, with twenty five samples yielding values below 1, ten samples with Q_n between 1 and 15, and four with Q_n higher than 100, with a maximum at 1100. Keeping these off-range values aside, mean $M_r = 0.267$ A m^{-1} and $Q_n = 0.875$ were obtained.

The orientation of M_r could be measured in 31 samples. Results were also rather variable, but for most of the window, a reverse magnetization with a relatively low inclination toward the N was found [*Ayarza et al*., 2017]. A mean orientation $I = -28º$, $D = 156º$ with a confidence limit of 9.9º for α_{95} probability was computed from 14 measurements in the central and southern part of the tectonic window, which is used to model all sections.

Samples in 12 sites yielded higher inclinations. These are mainly close to the coast, between Vilachá and Rúa, and showed mean values of $I = -61º$ and $D = 162º$ with a confidence limit of 9.5º for α_{95} probability was computed from 12 sampled sites. The change may be related with the structure of the antiform where the tectonic window crops out. Its axis plunges gently to the SSW in most of the antiform, but at the coast, it plunges to the NNE. A rotation about a WNW-ESE horizontal axis may explain the *c.* 30º change in the inclination of M_r. This

rotation can be related with movements of the faults of the same direction, which is also that of the coast. However, the possibility of a different magnetization affecting the coastal section in relation with the opening of the Biscay Bay should not be ruled out.

The orientation of M_r in the coastal region is not very different to that of the present Earth magnetic field used in the models (I = 58.6º, D = -2.5º), except for the fact that the M_r shows a reverse polarity. As the average Q_n is close to 1, this implies that M_r and M_i cancel each other to a significant amount, making modeling a difficult task. The fact that the anomaly in Section A is somewhat lesser than in the central and southern sections may suggest that the high inclination of M_r is meaningful.

For values of $Q_n > 0.1$, remanence is strong enough to be considered in modeling together with susceptibility. In our case, average Q_n approaches 1, meaning that contribution by M_r is comparable to that of M_i. Models including both magnetic susceptibility and remanence are shown in Figure 11. They use the same integer multiples of $\kappa = 0.01$ SI as in Figure 10, and multiples of $M_r = 0.267$ A m^{-1} with I = -28º, D = 156º for the remanence, except in Section A (1), where multiples of $\kappa = 0.0105$ and the values of M_r found close to the coast have been used: multiples of $M_r = 0.243$ A m^{-1} with I = -61º, D = 162º.

Figure 12 depicts the blocks of models that include only induced magnetization (a) and those that also consider remanent magnetization (b). The main differences between both groups of models, and the procedure followed for building the latter are:

- The effect of M_r is a displacement to the WNW of maxima and minima and a decrease in the anomaly amplitude. This is due to the reverse character of the remanent component, opposite to the normal polarity of the present Earth magnetic field, and is especially notorious when using the M_r values obtained close to the coast.
- To fit the observed anomaly, we have started from models in Figure 10 and tried different combinations of κ, M_r, and geometry of the blocks, making them bigger and displacing them toward the ESE. We might have changed the Königsberger ratio (Q_n) –the relationship between the remanent and induced components– since a decrease in Q_n (and M_r) increases the similarity between models with and without M_r. However, we have preferred to adhere to our statistical results and avoided the use of arbitrary M_r values, which would distort the aim of using geophysical data to constrain geology.
- The geometry of geological structures in the sections in Figure 11 needed to be partly modified with respect to those of Figure 10, in accordance with the requirements of M_r. This includes all sections but Section A, where the geometry has been kept the same for versions (1) and (2) to better compare with the result using the high-inclination values.
- The shape of the Middle Ordovician, magnetite-rich ironstone has been little modified in relation with the model without M_r, and in Section A (1), it is somewhat thicker to avoid increasing the values of κ and M_r, that was another possible option.
- The block of migmatites developed in the Vilalba Series has been kept with a $\kappa = 0.02$ SI, but its thickness has been slightly increased and/or its WNW limit displaced to the ESE.
- The block corresponding to the lower extensional shear zone has been kept with $\kappa = 0.04$ SI in Sections B, C and D, maintaining in Section C a couple of lenses with $\kappa = 0.06$ SI. However, κ was increased to 0.06 SI for the whole shear zone in Section A (2), and to 0.084 SI in Section A (1). Changes in thickness were made locally, but are significant in Sections A (2) and B, and very important in Section A (1). The block modeling the detachment joining the lower extensional shear zone in Sections A and B has been

merged with the shear zone in a single block with the same parameters. This implies increasing κ in the detachment to 0.084 SI in Section A (1), 0.06 SI in Section A (2) and 0.04 SI in Section B, and also making changes on its shape.

- The block modeling the reactivation of the Mondoñedo basal shear zone has been increased in susceptibility and/or thickness, except in Section B, where susceptibility has been halved, compensating the calculated anomaly by thickening the lower extensional shear zone.
- The block modeling the Viveiro shear zone has undergone changes in its geometry, increasing its westward dip from 15º-25º to 27º-50º, as a result of displacing its deeper parts to the ESE. Susceptibility was increased in Sections A (1) and B, but lowered in Sections A (2) and C.

5. Discussion

The ground-based magnetic map of the Xistral Tectonic Window shows complexities not revealed by the lower resolution aeromagnetic map of the Iberian Peninsula. Also, the new data provide clues for interpretation of the large arcuate aeromagnetic anomaly [*Ardizone et al*., 1989; *Miranda et al*., 1989] that occupies most of the NW quadrant of the Iberian Peninsula and delineates the Central Iberian Arc [*Martínez Catalán*, 2012], with the EGMA forming its northernmost part (Figure 1).

5.1. Highlights for the Xistral Tectonic Window

The relatively short wavelengths and high amplitude of the anomalies found in the newly acquired ground data have enabled us to model these features with bodies whose top is shallower than 1-3 km. Source rocks need to crop out, or nearly so, to match the anomalies in many cases. Magnetic bodies at depths greater than 5-8 km are not needed to explain the observed anomaly.

Rocks with high magnetic susceptibility (κ) crop out in the Xistral Tectonic Window, and are the main candidates for being the source of the anomaly. They are felsic rocks, including quartzites, schists, paragneisses, migmatites and inhomogeneous granites. The scarcity of basic and ultrabasic rocks at the surface, the weak or not magnetic character of these rocks, and the low value of the Bouguer anomaly above the tectonic window suggest that basic rocks do not represent significant magnetic sources.

Detailed magnetic surveying has also revealed that high κ values are not particular to any lithology, but appear in various types of high-grade metasedimentary rocks and their anatectic derivatives whenever they are associated with late Variscan extensional structures.

The Viveiro Fault and its associated shear zone seem responsible for the main anomaly, but other maxima have appeared at places where extensional detachments had been mapped. A major one occurs below the Lower Extensional Detachment, in a wide shear zone mostly occurring at its footwall beneath the Xistral Quartzite. This shear zone crops out in the central and N parts of the window. A magnetic maximum in the N, close to Vilachá, and two more in the center, at Viveiró (do not mistake with Viveiro) and 4 km to the S, occur where the detachment crops out (Figure 8), and are modeled by Sections A and C. In a broad strip *c.* 10 km N and S of Section B, the detachment is so close to the Viveiro Fault that the respective anomalies cannot be distinguished. However, in Section C, they are clearly separated. Due to the SSW plunge of the dome axis, the detachment does not crop out to the S, and Section D

shows only the maximum related with the Viveiro Fault. However, the assumed continuation of the detachment under the surface helps to adjust the models. Other subordinate magnetic maxima coincide with other detachments, as at Burela, or 8 km SW of Rúa.

An important question raised by this work is why magnetization is linked to extensional structures. Multidomain magnetite seems to be the primary carrier and responsible for the induced magnetization, while other iron oxides resulting from alteration, exsolution and replacement may be responsible for the remanence [*Ayarza et al.*, 2017]. The P-T paths of the inner parts of the Mondoñedo Nappe and the Lugo Dome draw a clockwise loop characterized by intermediate-P Barrovian metamorphism, followed by high-T and low-P, typical of collisional belts [*Martínez Catalán et al.*, 2014 and references therein]. The latter conditions reflect extensional collapse of the orogen that followed crustal thickening by recumbent folding and thrusting, and subsequent thermal relaxation. In the Xistral Tectonic Window, magnetite is a metamorphic mineral grown during decompression at high temperature, and inside the structures responsible for decompression.

Laboratory experiments have demonstrated that iron-rich rocks (goethite) with small amounts of organic matter may form magnetite after moderate reductive heating [*Till et al.*, 2015]. The main magnetic blocks in the model represent rocks from the Vilalba Series and Cándana Group, essentially consisting of metasediments derived from shale, quartzite and greywacke. The same stratigraphic ensembles crop out in low-grade parts of the Mondoñedo Nappe and its relative autochthon to the E, but there, magnetite was not found. Accordingly, magnetite was developed exclusively inside the extensional shear zones because these are characterized by high temperatures, relatively low pressures, and synkinematic recrystallization.

Growth of magnetite as a metamorphic phase is a petrological problem beyond the scope of this paper. It is worth noting, however, that magnetite is a typical mineral of contact metamorphism. Magnetite-rich ironstones of the Luarca Slates to the W of the Viveiro Fault, derived from sedimentary ooidal iron oxides originated in this way. Contact metamorphism in slates is characterized by high-T effects upon low-grade metamorphic rocks that were not deeply buried at the time of granite intrusion. So, the P-T conditions at which magnetite was formed by contact metamorphism are probably similar to those of the Lugo Dome during extensional collapse, although the previous evolution differs and no significant coeval deformation accompanies contact metamorphism.

The main outcome of the models presented in this paper is the spatial magnetic correspondence between the EGMA and the outcropping extensional structures. The contribution of the models to constrain the geometry of these structures is however limited by the inhomogeneous distribution of magnetic properties, only partially controlled at surface and fully unknown at depth. The models including magnetic remanence achieve a better fit, and not only because remanence is significant in the analyzed samples. A good example is the dip of the Viveiro Fault, which can be approximately established from S-C, or S-C' structures [*Platt*, 1984; *Blenkinsop and Treloar*, 1995; *Passchier and Trouw*, 1996]. Microshears in the Viveiro shear zone dip 45-60º W in the Viveiro area [*Martínez et al*., 1996], which agree better with the models including remanence (Figures 10 and 11).

5.2. The Curved Magnetic Anomaly at NW Iberia

According to the models, deep sources do not explain the waveforms of the ground-based magnetic anomaly in the Xistral Tectonic Window. Figure 13a shows the radially averaged power spectrum of the ground-based magnetic anomaly of the Xistral Tectonic Window and the depths estimated for the origin of the anomalies. Significant changes in the wavelength of

775 the anomalies are indicated by changes in the slope of the power spectrum, and allow the
776 separation of meaningful depths for the sources. The depths are then calculated in km
777 dividing by 4π the slope of the straight lines that fit different parts of the spectrum. In this
778 case, the results confirm the shallowness of the magnetic sources, the deepest of which lies at
779 4.1 km whereas other sources would be located at 1.8 km and 1.2 km (red, green and blue
780 lines respectively).

781 Deeper sources cannot be ruled out, however, because buried extensional detachments may
782 exist, and migmatites and associated granitoids could continue beneath 5 km, and could bear
783 ferrimagnetic components. In the central and southern parts of the Lugo Dome, the only
784 detachment cropping out is the Viveiro Fault, and no rocks with significant magnetic
785 susceptibility have been found. But the Lower Extensional Detachment and the migmatites
786 continue beneath the surface, buried due to the southward plunge of the dome axis. The same
787 holds for the Sanabria Dome, which forms the southern part of the EGMA.

788 The radially averaged power spectrum obtained for the whole EGMA using the aeromagnetic
789 data indicates wavelength components implying sources at 15.2, 7.1 and 2.9 km (Figure 13b),
790 although the height of flight above the surface (mean 2.6 km) must be subtracted. These
791 values should be taken as a reference, and comparison between the results from the two
792 datasets used in Figure 13 should be made with caution, because altitude and sampling
793 interval differ. For the EGMA spectrum, the uppermost and intermediate depths
794 (approximately 0.3 and 4.5 km once corrected) reflect sources at or close to the surface and
795 down to the maximum depth used in most of the 2D models presented here. So, they seem to
796 represent the contribution of the Xistral Tectonic Window. However, the deep sources
797 calculated in Figure 13b suggest that the migmatites and inhomogeneous granites continue
798 downward, reaching a depth of 12 km or more. The work of *Ayarza and Martínez Catalán*
799 [2007] modeled the aeromagnetic data set across the EGMA and addressed its origin at a
800 magmatic lens shaped body outcropping in the Xistral window but reaching mid crustal
801 depths. The aeromagnetic anomaly (Figure 9b) is wider than the upward continuation of the
802 ground level map (Figure 9a) probably because the latter is less sensitive to the effect of deep
803 structures, as it has a higher sampling rate and covers a smaller area.

804 The EGMA coincides with the Lugo and Sanabria Domes. Deep extension-related sources
805 probably account for other magnetic anomalies occurring in the continuation of the EGMA
806 toward central Spain, coinciding with the Tormes and Gredos Domes. From the latter, the
807 anomaly turns to the W and NW in central and northern Portugal, through the Ciudad Rodrigo
808 Dome, a series of granitic batholiths around Guarda and finally the granitic and migmatitic
809 Porto-Viseu Belt (Figure 1a). In fact, magnetite was developed in the latter during
810 migmatization, and the rocks there are characterized by high magnetic susceptibilities and
811 thermal remanent magnetization [*Ribeiro et al*., 2015].

812 The curved shape of the broad magnetic anomaly closely follows the alignment defined by the
813 domes and together, they delineate the core of the Central Iberian Arc (Figure 1b). Moreover,
814 the magnetic anomaly surrounds the Galicia-Trás-os-Montes Zone (GTMZ), which represents
815 the preserved part of a large and thick allochthonous nappe stack. It is thought that dome
816 development followed crustal thickening, largely induced by nappe emplacement. And both
817 the domes and the anomaly reflect the shape of the Allochthon [*Martínez Catalán et al*., 2014;
818 *Alcock et al*., 2015]. Actually, other domes occur among the allochthonous complexes
819 (Celanova, Padrón and Peares; Figure 1a), confirming that they developed under the nappe
820 pile, and positive magnetic anomalies occur at the Padrón Dome (Figure 1).

821

6. Conclusions

A ground-based magnetic map has been acquired in an extensional, late Variscan structural and metamorphic dome coinciding with the Eastern Galicia Magnetic Anomaly (EGMA). Our survey covers the Xistral Tectonic Window, where the relative autochthon of the Mondoñedo thrust sheet outcrops.

The new map shows anomalies with relatively short wavelength and high amplitude that need to be modeled with shallow magnetic bodies. The maxima coincide with outcrops of previously identified extensional shear zones associated with late Variscan detachments. The two most important ones are the Viveiro Fault and the Lower Extensional Detachment, whose ductile shear zones are a few kilometers thick. They both are responsible for the highest amplitude anomalies.

Magnetic properties are essentially linked to high-grade metasedimentary rocks deformed in late Variscan extensional structures, and in their anatectic derivatives. Large metamorphic grains of magnetite occur in Lower Cambrian and Neoproterozoic quartzites, schists, paragneisses, migmatites and inhomogeneous granites, and are responsible for the induced magnetization, while secondary iron oxides may be responsible for remanence. Outcropping basic and ultrabasic rocks are scarce and poorly magnetized, and the low value of the Bouguer gravity anomaly indicates that they are not volumetrically important at depth.

2D modeling was carried out using only induced magnetization and also including magnetic remanence. The models support the relationship of the magnetic anomalies with extensional structures. Models including remanence seem more accurate, as they match better the geometry of large structures such as the Viveiro Fault. However, the ability of the models to constrain the geometry of the structures in detail is limited by the inhomogeneous and largely unknown distribution of magnetic properties in the shear zones at depth.

Sources deeper than *c.* 5 km are not needed to explain the waveforms of the ground-based magnetic anomaly in the Xistral Tectonic Window, but they exist, as indicated by the radially averaged power spectrum of the aeromagnetic dataset. No outcropping extensional detachments, continuation of those identified at the tectonic window and even deeper ones probably occur in the central and southern parts of the EGMA, down to depths of 12 km or more.

The continuation of the EGMA by a broad anomaly to the S and SE until central Spain, and then to the W and NW in Portugal, also overlaps extensional structures, either cropping out or buried. Accordingly, we hereby relate magnetic anomalies at the core of the Central Iberian Arc with migmatitic domes and/or with large granitic batholiths below which large migmatitic domains could be expected. The age of magnetization could shed some light on the timing of tectonics events in the Iberian Massif.

Finally, the existence of metasediments in an extensional tectonics setting has been addressed as an important source of magnetization. Similar structures should be searched for and identified worldwide in an effort to understand magnetization processes.

Acknowledgements. This contribution has been funded by the research projects CGL2011-22728 of the Spanish Ministry of Science and Innovation, CGL2016-78560-P and CGL2016-77560 of the Spanish Ministry of Economy, Industry and Competitiveness, as part of the National Program of Promotion of Scientific and Technical Research of Excellence, in the frame of the National Plan of Scientific and Technical Research and Innovation 2013-2016, and by research project SA065P17 from the regional government (Junta de Castilla y León).

The two first and the last projects provided funds for all authors except JJV, whose research was covered by the third project. The Bouguer gravity anomaly data can be downloaded from the Bureau Gravimétrique International (BGI), http://bgi.obs-mip.fr, previous request, and for NW Spain they were compiled by A. Casas and V. Pinto, of the Departamento de Geoquímica, Petrología y Prospección Geofísica, Universidad de Barcelona, whose contribution is acknowledged. Data of the aeromagnetic map of Spain are property of the Instituto Geográfico Nacional (IGN), www.ign.es/web/ign/portal, and can be obtained under request. We thank I. Socías, of the Instituto Geográfico Nacional, and J. M. Miranda, of the Centro de Geofisica da Universidade de Lisboa, for providing the data used in plotting the aeromagnetic map of the Iberian Peninsula. Supporting information: Table S1 includes ground-level data; Table S2 includes values of magnetic susceptibility measured *in situ*. The rest of the data used are listed in the references. Jean-Bernard Edel and Christine Syddoway are acknowledged for their careful insights of the manuscript, allowing us to significantly improve the final version.

References

Aerden, D. G. A. M. (2004), Correlating deformation in Variscan NW-Iberia using porphyroblasts; implications for the Ibero-Armorican Arc, *J. Struct. Geol.*, *26*, 177–196.

Alcock, J. E., J. R. Martínez Catalán, R. Arenas, and A. Díez Montes (2009), Use of thermal modelling to assess the tectono-metamorphic history of the Lugo and Sanabria gneiss domes, Northwest Iberia, *Bull. Soc. Géol. France*, *180*, 179–197.

Alcock, J. E., J. R. Martínez Catalán, F.J. Rubio Pascual, A. Díez Montes, R. Díez Fernández, J. Gómez Barreiro, R. Arenas, I. Dias da Silva, and E. González Clavijo (2015), 2-D thermal modeling of HT-LP metamorphism in NW and Central Iberia: Implications for Variscan magmatism, rheology of the lithosphere and orogenic evolution. *Tectonophysics*, *657*, 21–37, doi:10.1016/j.tecto.2015.05.022.

Aller, J. (1986), Una hipótesis sobre la estructura geológica profunda causante de la anomalía magnética regional de una parte del área del Manto de Mondoñedo, *Brev. Geol. Astúrica*, *28*, 4–12.

Aller, J., and F. Bastida (1993), Anatomy of the Mondoñedo Nappe basal shear zone (NW Spain), *J. Struct. Geol.*, *15*, 1405–1419.

Aller, J., H. J. Zeyen, A. Pérez-Estaún, J. A. Pulgar, and J. M. Parés (1994), A 2.5D interpretation of the eastern Galicia magnetic anomaly (northwestern Spain): geodynamical implications, *Tectonophysics*, *237*, 201–213.

Álvarez-Marrón, J., A. Pérez-Estaún, J. J. Dañobeitia, J. A. Pulgar, J. R. Martínez Catalán, A. Marcos, F. Bastida, J. Aller, P. Ayarza Arribas, J. Gallart, F. González-Lodeiro, E. Banda, M. C. Comas, and D. Córdoba (1995), Results from ESCI-N3.1 and ESCI-N3.2 marine deep seismic profiles in the northwestern Galicia Margin, *Rev. Soc. Geol. España*, *8*, 331–339.

Alvarez-Marrón, J., A. Pérez-Estaún, J. J. Dañobeitia, J. A. Pulgar, J. R. Martínez Catalán, A. Marcos, F. Bastida, P. Ayarza Arribas, J. Aller, J. Gallart, F. González-Lodeiro, E. Banda, M. C. Comas, and D. Córdoba (1996), Seismic structure of the northern continental margin of Spain from ESCIN deep seismics profiles, *Tectonophysics*, *264*, 153–174.

913 Ardizone García, J. A. (1998), Análisis de datos aeromagnéticos. Metodologías y aplicación
914 al levantamiento aeromagnético de España peninsular. *Instituto Geográfico Nacional,*
915 *Publ. Técn.*, *32*, 228 pp.

916 Ardizone, J., J. Mezcua, and I. Socías (1989), *Mapa aeromagnético de España peninsular*,
917 Escala 1:1.000.000, Instituto Geográfico Nacional, Madrid.

918 Arenas, R., and J. R. Martínez Catalán (2003), Low-P metamorphism following a Barrovian-
919 type evolution. Complex tectonic controls for a common transition, as deduced in the
920 Mondoñedo thrust sheet (NW Iberian Massif), *Tectonophysics*, *365*, 143–164.

921 Arenas, R., J. R. Martínez Catalán, S. Sánchez Martínez, F. Díaz García, J. Abati, J.
922 Fernández-Suárez, P. Andonaegui, and J. Gómez-Barreiro (2007), Paleozoic ophiolites
923 in the Variscan suture of Galicia (northwest Spain): distribution, characteristics and
924 meaning, in *4-D evolution of continental crust, Geol. Soc. Am. Mem.*, vol. 200, edited
925 by R. D. Hatcher Jr., M. P. Carlson, J. H. McBride, and J. R. Martínez Catalán, pp.
926 425–444, doi:10.1130/2007.1200(22), GSA, Boulder, Co.

927 Arenas, R., S. Sánchez Martínez, R. Díez Fernández, A. Gerdes, J. Abati, J. Fernández-
928 Suárez, P. Andonaegui, P. González Cuadra, A. López Carmona, R. Albert, J. M.
929 Fuenlabrada, and F. J. Rubio Pascual (2016), Allochthonous terranes involved in the
930 Variscan suture of NW Iberia: A review of their origin and tectonothermal evolution,
931 *Earth-Sci. Rev., 161*, 140–178, doi: 10.1016/j.earscirev.2016.08.010.

932 Ayarza, P., and J. R. Martínez Catalán (2007), Potential field constraints on the deep structure
933 of the Lugo gneiss dome (NW Spain), *Tectonophysics*, *439*, 67–87,
934 doi:10.1016/j.tecto.2007.03.007.

935 Ayarza, P., J. R. Martínez Catalán, J. Gallart, J. J. Dañobeitia, and J. A. Pulgar (1998),
936 Estudio Sísmico de la Corteza Ibérica Norte 3.3: a seismic image of the Variscan crust
937 in the hinterland of the NW Iberian Massif, *Tectonics*, *17*, 171–186.

938 Ayarza, P., J. R. Martínez Catalán, J. Álvarez-Marrón, H. Zeyen, and C. Juhlin (2004),
939 Geophysical constraints on the deep structure of a limited ocean-continent subduction
940 zone at the north Iberian margin, *Tectonics, 23 (1)*, 1–21, TC1010,
941 doi:10.1029/2002TC001487.

942 Ayarza, P., J. R. Martínez Catalán, J. J. Villalaín, F. Alvarez Lobato, M. Durán-Oreja, and C.
943 Prada-Galende (2017), Characterizing the Eastern Galicia Magnetic Anomaly (NW
944 Spain): Origin of the mineralization and implications on the age of the Central Iberian
945 Arc, *EGU2017-6816*, Viena.

946 Bastida, F., J. R. Martínez Catalán, and J. A. Pulgar (1986), Structural, metamorphic and
947 magmatic history of the Mondoñedo nappe (Hercynian belt, NW Spain), *J. Struct.*
948 *Geol.*, *8*, 415–430.

949 Blenkinsop, T. G., and P. J. Treloar (1995), Geometry, classification and kinematics of S-C
950 and S-C' fabrics in the Mushandike area, Zimbabwe, *J. Struct. Geol*., *17*, 397–408.

951 Block, L., and L. H. Royden (1990), Core complex geometries and regional scale flow in the
952 lower crust, *Tectonics*, *9*, 557–567.

953 Capdevila, R. (1966), Sur la présence de sills basiques et ultrabasiques métamorphisés dans la
954 région de Villalba (Lugo, Espagne), *C. R. Acad. Sci. Paris*, *262*, 2193–2196.

955 Capdevila, R. (1969), *Le métamorphisme régional progressif et les granites dans le segment*
956 *hercynien de Galice nord oriental (NW de l'Espagne)*, Ph. D. Thesis, University of
957 Montpellier. 430 pp.

958 Coney, P. J., and T. A. Harms (1984), Cordilleran metamorphic core complexes: Cenozoic
959 extension of Mesozoic compression, *Geology*, *12*, 550–554.

960 Dallmeyer, R. D., J. R. Martínez Catalán, R. Arenas, J. I. Gil Ibarguchi, G. Gutiérrez Alonso,
961 P. Farias, J. Aller, and F. Bastida (1997), Diachronous Variscan tectonothermal
962 activity in the NW Iberian Massif: Evidence from $^{40}Ar/^{39}Ar$ dating of regional fabrics,
963 *Tectonophysics*, *277*, 307–337.

964 de Poulpiquet, J. (2012), L'arc magnétique ibéro-armoricain est-il la trace d'un rift avorté
965 d'âge cambro-ordovicien? *Trab. Geol.*, *Univ. Oviedo*, *32*, 76–86.

966 Dias da Silva, I., P. Valverde-Vaquero, E. González-Clavijo, A. Díez-Montes, A., and J. R.
967 Martínez Catalán (2014a), Structural and stratigraphical significance of U-Pb ages
968 from the Mora and Saldanha volcanic complexes (NE Portugal, Iberian Variscides), in
969 *The Variscan Orogeny: Extent, Timescale and the Formation of the European Crust*,
970 *Geol. Soc. London, Spec. Publ.*, vol. 405, edited by K. Schulmann, J. R. Martínez
971 Catalán, J. M. Lardeaux, V. Janousek, and G. Oggiano, pp. 115–135,
972 doi:10.1144/SP405.3.

973 Dias da Silva, Í., U. Linnemann, M. Hofmann, E. González Clavijo, A. Díez-Montes, and J.
974 R. Martínez Catalán (2014b), Detrital zircon and tectonostratigraphy of the
975 Parautochthon under the Morais Complex (NE Portugal): implications for the Variscan
976 accretionary history of the Iberian Massif, *J. Geol. Soc. London*, *172*, 45–61,
977 doi:10.1144/jgs2014-005.

978 Díaz García, F., J. R. Martínez Catalán, R. Arenas, and P. González Cuadra (1999), Structural
979 and kinematic analysis of the Corredoiras Detachment: evidence for early variscan
980 orogenic extension in the Ordenes Complex, NW Spain, *Int. J. Earth Sci., 88*, 337–
981 351.

982 Díez Fernández, R., J. R. Martínez Catalán, J. Gómez Barreiro, and R. Arenas (2012),
983 Extensional flow during gravitational collapse: A tool for setting plate convergence
984 (Padrón migmatitic dome, Variscan belt, NW Iberia), *J. of Geology, 120 (1)*, 83–103,
985 doi: 10.1086/662735.

986 Díez Montes, A., J. R. Martínez Catalán, and F. Bellido Mulas (2010), Role of the Ollo de
987 Sapo massive felsic volcanism of NW Iberia in the Early Ordovician dynamics of
988 northern Gondwana. *Gondwana Res.*, *17*, 363–376, doi:10.1016/j.gr.2009.09.001.

989 Eskola, P. E. (1949), The problem of mantled gneiss domes, *Geol. Soc. London, Quart. J.,*
990 *104*, 461–476.

991 Farias, P., G. Gallastegui, F. González-Lodeiro, J. Marquínez, L. M. Martín Parra, J. R.
992 Martínez Catalán, J. G. de Pablo Maciá, and L. R. Rodríguez Fernández (1987),
993 Aportaciones al conocimiento de la litoestratigrafía y estructura de Galicia Central,
994 *Mem. Fac. Ciências, Univ. Porto*, *1*, 411–431.

995 Fernández-Suárez, J., G. R. Dunning, G. A. Jenner, and G. Gutiérrez-Alonso (2000), Variscan
996 collisional magmatism and deformation in NW Iberia: constraints from U-Pb
997 geochronology of granitoids. *J. Geol. Soc., London*, *157*, 565–576.

Fisher, G. W., and S. N. Olsen (2004), The Baltimore Gneiss domes of the Maryland Piedmont, in *Gneiss domes in orogeny, Geol. Soc. Am. Spec. Paper*, vol. 380, edited by D. L. Whitney, C. Teyssier, C., and C. Siddoway, pp. 307–320, GSA, Boulder, Co.

Franke, W., and E. Stein (2000), Exhumation of high-grade rocks in the Saxo-Thuringian Belt: geological constraints and geodynamic concepts, in *Orogenic Processes: Quantification and Modelling in the Variscan Belt*, *Geol. Soc. London, Spec. Publ.*, vol. 179, edited by W. Franke, V. Haak, O. Oncken, and D. Tanner, pp. 337-354.

Gabriel, G., D. Vogel, R. Scheibe, H. Lindner, R. Pucher, T. Wonik, and C. M. Krawczyk (2011), Anomalies of the Earth's total magnetic field in Germany – the first complete homogeneous data set reveals new opportunities for multiscale geoscientific studies, *Geophys. J. Int.*, *184*, 1113–1118, doi: 10.1111/j.1365-246X.2010.04924.x.

Galán, G. (1987), Las rocas graníticas del Macizo de Vivero en el sector Norte (Lugo, NO de España), *Corpus Geol. Gallaeciae*, *2ª Serie*, *3*, 376 pp.

Gómez Barreiro, J., J. R. Martínez Catalán, R. Díez Fernández, R., Arenas, and F. Díaz García (2010), Upper crust reworking during gravitational collapse: the Bembibre-Pico Sacro detachment system (NW Iberia), *J. Geol. Soc., London, 167*, 769–784, doi: 10.1144/0016-76492009-160.

Gutiérrez-Alonso, G., J. Fernández-Suárez, D. Pastor-Galán, S. T. Johnston, U. Linnemann, M. Hofmann, J. Shaw, J. R. Colmenero, and P. Hernández (2015), Significance of detrital zircons in Siluro-Devonian rocks from Iberia, *J. Geol. Soc. London*, *172*, 309–322, doi:10.1144/jgs2014–118.

Gutiérrez Marco, J. C., and I. Rábano (2015), Hierros sedimentarios ordovícicos y patrimonio minero de Viveiro (Lugo), *De Re Metallica*, 23, 1–37.

Harwood, D. D. and I. Zietz (1974), Configuration of Precambrian rocks in southeastern New York and adjacent New England from aeromagnetic data, *Geol. Soc. Am. Bull.*, *85*, 181–188.

Higgins, M. W., G. W. Fisher, and I. Zietz (1973), Aeromagnetic discovery of a Baltimore gneiss dome in the Piedmont of Northwestern Delaware and Southeastern Pennsylvania, *Geology*, *1*, 41–43, reproduced in GEOLOGY Rerun, *GSA Today*, *25* (9), 5–7, doi: 10.1130/0091-7613(1973)1<41:ADOABG>2.0.CO;2.

Instituto Geográfico Nacional (1975), *Mapa Geomagnético de España (España Peninsular y Baleares). Isodinámicas Totales*. Escala: 1:1.000.000. Madrid.

Instituto Geográfico Nacional (1987), *Mapa aeromagnético de España peninsular (campo residual)*. Escala 1: 1.000.000. Ministerio de Obras Públicas y Urbanismo.

Instituto Geográfico Nacional (1996), *Anomalías gravimétricas Bouguer de la Península Ibérica y Baleares*. Escala 1/1.000.000. Madrid.

Lister, G. S., and G. A. Davis (1989), The origin of metamorphic core complexes and detachment faults formed during Tertiary continental extension in the northern Colorado River region, U.S.A., *J. Struct. Geol.*, *11*, 65–94.

Llopis Lladó, N. (1966), Sur la structure hercynienne de l'Espagne et ses rapports avec la Chaîne hercynienne en Europe occidentale, *C. R. Séances, Acad. Sci., Paris*, Série D, *262*, 2581–2584.

Lunar Hernández, R. (1977), Mineralogénesis de los yacimientos de hierro del Noroeste de la Península, *Mem. Inst. Geol. Min. España*, *90*, 211 pp.

1042 Martínez, F. J., J. Carreras, M. L. Arboleya, and C. Dietsch (1996), Structural and
1043 metamorphic evidence of local extension along the Vivero fault coeval with bulk
1044 crustal shortening in the Variscan chain (NW Spain), *J. Struct. Geol*., *18*, 61–73.

1045 Martínez Catalán, J. R. (2012), The Central Iberian arc, an orocline centred in the Iberian
1046 Massif and some implications for the Variscan belt, *Int. J. Earth Sci*., *101*, 1299–1314,
1047 doi:10.1007/s00531-011-0715-6.

1048 Martínez Catalán, J. R., P. Ayarza Arribas, J. A. Pulgar, A. Pérez-Estaún, J. Gallart, A.
1049 Marcos, F. Bastida, J. Álvarez-Marrón, F. González Lodeiro, J. Aller, J. J. Dañobeitia,
1050 E. Banda, D. Cordoba, and M. C. Comas (1995), Results from the ESCI-N3.3 marine
1051 deep seismic profile along the Cantabrian continental margin, *Rev. Soc. Geol. España*,
1052 *8*, 341–354.

1053 Martínez Catalán, J. R., R. Arenas, F. Díaz García, F. J. Rubio Pascual, J. Abati, and J.
1054 Marquínez (1996), Variscan exhumation of a subducted Paleozoic continental margin:
1055 The basal units of the Ordenes Complex, Galicia, NW Spain, *Tectonics, 15*, 106–121.

1056 Martínez Catalán, J. R., F. Díaz García, R. Arenas, J. Abati, P. Castiñeiras, P. González
1057 Cuadra, J. Gómez Barreiro, and F. Rubio Pascual (2002), Thrust and detachment
1058 systems in the Ordenes Complex (northwestern Spain): Implications for the Variscan-
1059 Appalachian geodynamics, in *Variscan-Appalachian Dynamics: the Building of the*
1060 *Late Paleozoic Basement, Geol. Soc. Am. Spec. Paper*, vol. 364, edited by J. R.
1061 Martínez Catalán, R. D. Hatcher Jr., R. Arenas, and F. Díaz García, pp. 163–182,
1062 GSA, Boulder, Co.

1063 Martínez Catalán, J. R., R. Arenas, and M. A. Díez Balda (2003), Large extensional structures
1064 developed during emplacement of a crystalline thrust sheet: the Mondoñedo nappe
1065 (NW Spain), *J. Struct. Geol.*, *25*, 1815–1839.

1066 Martínez Catalán, J. R., J. Fernández-Suárez, G. A. Jenner, E. Belousova, and A. Díez Montes
1067 (2004), Provenance constraints from detrital zircon U-Pb ages in the NW Iberian
1068 Massif: implications for Paleozoic plate configuration and Variscan evolution, *J. Geol.*
1069 *Soc. London*, *161*, 461–473.

1070 Martínez Catalán, J. R., R. Arenas, F. Díaz García, J. Gómez-Barreiro, P. Gónzalez Cuadra, J.
1071 Abati, P. Castiñeiras, J. Fernández-Suárez, S. Sánchez Martínez, P. Andonaegui, E.
1072 Gónzalez Clavijo, A. Díez Montes, F. J. Rubio Pascual, and B. Valle Aguado (2007),
1073 Space and time in the tectonic evolution of the northwestern Iberian Massif.
1074 Implications for the comprehension of the Variscan belt, in *4-D evolution of*
1075 *continental crust, Geol. Soc. Am. Mem.*, vol. 200, edited by R. D. Hatcher Jr., M. P.
1076 Carlson, J. H. McBride, and J. R. Martínez Catalán, pp. 403–423,
1077 doi:10.1130/2007.1200(21), GSA, Boulder, Co.

1078 Martínez Catalán, J. R., J. Fernández-Suárez, C. Meireles, E. González Clavijo, E. Belousova,
1079 and A. Saeed (2008), U–Pb detrital zircon ages in synorogenic deposits of the NW
1080 Iberian Massif (Variscan belt): interplay of Devonian-Carboniferous sedimentation
1081 and thrust tectonics, *J. Geol. Soc. London*, *165*, 687–698.

1082 Martínez Catalán, J. R., R. Arenas, J. Abati, S. Sánchez Martínez, F. Díaz García, J.
1083 Fernández-Suárez, P. González Cuadra, P. Castiñeiras, J. Gómez Barreiro, A. Díez
1084 Montes, E. González Clavijo, F. J. Rubio Pascual, P. Andonaegui, T. E. Jeffries, J. E.
1085 Alcock, R. Díez Fernández, and A. López Carmona (2009), A rootless suture and the
1086 loss of the roots of a mountain chain: the Variscan belt of NW Iberia. *C. R.*
1087 *Geoscience*, *341*, 114–126, doi:10.1016/j.crte.2008.11.004.

1088 Martínez Catalán, J. R., F. Álvarez Lobato, V. Pinto, J. Gómez Barreiro, P. Ayarza, J. J.
1089 Villalaín, and A. Casas (2012), Gravity and magnetic anomalies in the allochthonous
1090 Órdenes Complex (Variscan belt, NW Spain): Assessing its internal structure and
1091 thickness, *Tectonics*, *31*, TC5007, 1–18, doi:10.1029/2011TC003093.

1092 Martínez Catalán, J. R., F. J. Rubio Pascual, A. Díez Montes, R. Díez Fernández, J. Gómez
1093 Barreiro, I. Dias da Silva, E. González Clavijo, P. Ayarza, and J. E. Alcock (2014),
1094 The late Variscan HT/LP metamorphic event in NW and Central Iberia: relationships
1095 to crustal thickening, extension, orocline development and crustal evolution, in *The*
1096 *Variscan Orogeny: Extent, Timescale and the Formation of the European Crust*, *Geol.*
1097 *Soc. London, Spec. Publ.*, vol. 405, edited by K. Schulmann, J. R. Martínez Catalán, J.
1098 M. Lardeaux, V. Janousek, and G. Oggiano, pp. 225–247, doi:10.1144/SP405.1.

1099 Matte, Ph. (1968), La structure de la virgation hercynienne de Galice (Espagne). *Rev. Géol.*
1100 *Alpine*, *44*, 1–128.

1101 Mezcua, J., A. Gil, and R. Benarroch (1996), *Estudio gravimétrico de la Península Ibérica y*
1102 *Baleares*, Instituto Geográfico Nacional, Madrid, 7 pp.

1103 Miranda, J. M., A. Galdeano, J. C. Rossignol, and L. A. Mendes Victor (1989), Aeromagnetic
1104 anomalies in mainland Portugal and their tectonic implications, *Earth Planet. Sci.*
1105 *Lett.*, *95*, 161–172.

1106 Parga-Pondal, I., P. Matte, and R. Capdevila (1964), Introduction à la géologie de l'"Ollo de
1107 Sapo", Formation porphyroide antesilurienne du Nord Ouest de l'Espagne, *Not. Com.*
1108 *Inst. Geol. Min. España*, *76*, 119–153.

1109 Passchier, C. W., and R. A. J, Trouw (1996), *Microtectonics*, Springer, Berlin, 289 pp.

1110 Pérez-Estaún, A., F. Bastida, J. L. Alonso, J. Marquínez, J. Aller, J. Álvarez-Marrón, A.
1111 Marcos, and J. A. Pulgar (1988), A thin-skinned tectonics model for an arcuate fold
1112 and thrust belt: The Cantabrian Zone (Variscan Ibero-Armorican Arc), *Tectonics, 7*,
1113 517–537.

1114 Pérez-Estaún, A., J. A. Pulgar, E. Banda, J. Álvarez-Marrón, and ESCI-N Research Group
1115 (1994), Crustal structure of the external Variscides in NW Spain from deep seismic
1116 reflection profiling, *Tectonophysics*, *232*, 91–118.

1117 Pérez-Estaún, A., J. A. Pulgar, J. Álvarez-Marrón, and ESCI-N group (1997), Crustal
1118 structure of the Cantabrian Zone: seismic image of a Variscan foreland thrust and fold
1119 belt (NW Spain), *Rev. Soc. Geol. España*, *8*, 307–319.

1120 Platt, J. P. (1984), Secondary cleavages in ductile shear zones, *J. Struct. Geol*., 6, 439–442.

1121 Pulgar, J. A., J. Gallart, G. Fernández-Viejo, A. Pérez-Estaún, J. Álvarez-Marrón, and ESCIN
1122 Group (1996), Seismic image of the Cantabrian Mountains in the western extension of
1123 the Pyrenees from integrated ESCIN reflection and refraction data, *Tectonophysics*,
1124 *264*, 1–19.

1125 Ribeiro, M. A., M. Areias, J. Ferreira, H. Martins, and H. Sant'Ovaia (2015), Geological and
1126 petrological constraints on the variscan evolution of the NW area of the Port-Viseu
1127 Belt, in *The Variscan belt: correlations and plate dynamics. Géologie de la France*
1128 *2015*, *1*, p. 150.

1129 Robardet, M. (2003), The Armorica 'microplate': fact or fiction? Critical review of the
1130 concept and contradictory paleobiogeographical data, *Palaeogeogr. Palaeoclim.*
1131 *Palaeoecol*., *195*, 125–148.

1132 Sánchez Martínez, S., R. Arenas, F. Díaz García, J. R. Martínez Catalán, J. Gómez-Barreiro,
1133 and J. A. Pearce (2007), The Careón Ophiolite, NW Spain: Supra-subduction zone
1134 setting for the youngest Rheic Ocean floor, *Geology*, *35*, 53–56.

1135 Shaw, J., G. Gutiérrez-Alonso, S. T. Johnston, and D. Pastor Galán (2014), Provenance
1136 variability along the Early Ordovician north Gondwana margin: Paleogeographic and
1137 tectonic implications of U-Pb detrital zircon ages from the Armorican Quartzite of the
1138 Iberian Variscan belt. *Geol. Soc.Am. Bull.*, *126*, 702–719, doi:10.1130/B30935.1.

1139 Staub, R. (1926), Gedanken zum Strukturbild Spaniens, *Vierteljs. des Naturf. Ges. Zürich*, *71*,
1140 196–260.

1141 Staub, R. (1928), Gedanken zum Strukturbild Spaniens, *Extrait des Comptes-Rendus, XIV*
1142 *Congrès Géologique International, 1926*, Gráficas Reunidas, Madrid, 50 pp.

1143 Thompson, G. A., and J. McCarthy (1990), A gravity constraint on the origin of highly
1144 extended terranes, *Tectonophysics*, *174*, 197–206.

1145 Till, J. L., Y. Guyodo, F. Lagroix, G. Morin, and G. Ona-Nguema (2015), Goethite as a
1146 potential source of magnetic nanoparticles in sediments, *Geology*, *43*, 75–78.

1147 Tirel, C., J. P. Brun, and E. Burov (2004), Thermomechanical modeling of extensional gneiss
1148 domes, in *Gneiss domes in orogeny*, *Geol. Soc. Am. Spec. Paper*, vol. 380,edited by D.
1149 L. Whitney, C. Teyssier, and C. S. Siddoway, pp. 67–78, GSA, Boulder, Co.

1150 Vanderhaeghe, O. (2004), Structural development of the Naxos migmatite dome, in *Gneiss*
1151 *domes in orogeny, Geol. Soc. Am. Spec. Paper*, vol. 380, edited by D. L. Whitney, C.
1152 Teyssier, and C. S. Siddoway, pp. 211–227, GSA, Boulder, Co.

1153 Whitney, D. L., C. Teyssier, and O. Vanderhaeghe (2004), Gneiss domes and crustal flow, in
1154 *Gneiss domes in orogeny, Geol. Soc. Am. Spec. Paper*, vol. 380, edited by D. L.
1155 Whitney, C. Teyssier, and C. S. Siddoway, pp. 15–33, GSA, Boulder, Co.

1156 Yin, A. (2004), Gneiss domes and gneiss dome systems, in *Gneiss domes in orogeny, Geol.*
1157 *Soc. Am. Spec. Paper*, vol. 380, edited by D. L. Whitney, C. Teyssier, and C. S.
1158 Siddoway, pp. 1–14, GSA, Boulder, Co.

1159 Zietz, I., R. T. Haworth, H. Williams, and D. L. Daniels (1980), *Magnetic anomaly map of the*
1160 *Appalachian Orogen*, Memorial University of Newfoundland, Map NO. 2a, scale 1:
1161 2,000,000.

1162

1163 # Tables

1164 Table 1. Model parameters and significant magnetic values

Densities for the Bouguer anomaly model	
Bouguer correction	2670 kg m^{-3}
Cabo Ortegal Complex	2860-2870 kg m^{-3}
Ophiolites of Cabo Ortegal and Órdenes complexes	2870 kg m^{-3}
Low-grade Cambro-Ordovician slates	2790 kg m^{-3}
Xistral Quartzite	2630 kg m^{-3}
Migmatites	2650 kg m^{-3}
A Tojiza granodiorite	2670 kg m^{-3}
Upper and middle crust	2670 kg m^{-3}
Lower crust	2900 kg m^{-3}
Mantle	3260 kg m^{-3}
Magnetic acquisition and processing data	
Base station for diurnal and secular corrections	UTM Zone 29: E613923, N4832265, 141 m
Reference date for corrections	April 14th, 2015
IGRF of base station at the reference date	B = 45861 nT, I = 58.72º, D = -2.537º
Corrected maximum and minimum values	777 and -437 nT
Maximum and minimum values of gridded data	737 and -403 nT
Parameters for the magnetic models	
Mean susceptibility of drilled samples	κ = 0.0099 SI
Mean susceptibility of the coastal section	κ = 0.00105 SI
Earth's magnetic field used in the models	B = 45817.6 nT, I = 58.6º, D = -2.5º
Susceptibilities used in model blocks	Multiples of κ = 0.01 SI
Maximum and minimum values used	0.08 and 0.02 SI; 0.001 SI in granodiorite
Exception: Figure 10, Section A (1)	Multiples of κ = 0.0105 SI; 0.084 and 0.021 SI
Field H used for magnetic induction ($M_i = \kappa H$)	36.1186 A m^{-1}
Magnetic remanence (M_r) used in models	Multiples of 0.267 A m^{-1} (the same used for κ)
Orientation of M_r	I = -28º, D = 156º
Exception: M_r for Section A (1) in Figure 10	Multiples of 0.243 A m^{-1} (the same used for κ)
Orientation of M_r for Section A (1) in Figure 10	I = -61º, D = 162º

1165

1166

Figure captions

Figure 1. (a) Map showing the outcrops of the Variscan basement in the Iberian Peninsula and the subdivision in zones of the Iberian Massif. Gneiss domes around the allochthonous complexes and the main strike-slip shear zones are included. Dashed purple lines approximately separate zones in areas covered by Mesozoic and Cenozoic sediments. Blue lines show the position of seismic profiles in Figure 2b. Abbreviations: CIA: Central Iberian Arc; IAA: Ibero-Armorican Arc. Gneiss domes: CR: Ciudad Rodrigo; Ce: Celanova; Gd: Guadarrama; Gr: Gredos; Gu: Guitiriz; Lu: Lugo; Pa: Padrón; Pe: Peares; Sa: Sanabria; Tr: Tormes; PV: Porto-Viseu. Strike-slip shear zones: BCSZ: Badajoz-Córdoba; DBSZ: Douro-Beira; JPSZ: Juzbado-Penalva; PTSZ: Porto-Tomar; SISZ: Southern Iberian. (b) Aeromagnetic map of the Iberian Peninsula. Data from *Ardizone et al*. [1989] for Spain and *Miranda et al*. [1989] for Portugal.

Figure 2. (a) Geological section across NW Iberia showing the major contractional and extensional structures and above, the age of deformation episodes along the section. C1: recumbent folding; C2: thrusting; C3: upright folding and ductile wrenching; E1 and E2: extension, characterized by detachments and domes. (b) Composite seismic section built from vertical incidence seismic reflection profiles from NW Iberia, and representing approximately the equivalent parts of the geological section (profiles ESCIN 1.1, 1.2, 3.2 and 3.3). Thin red lines mark limits of reflection packages, and the lowermost line in each part of the section represents the Moho, assumed to occur at the base of one or more bands of reflective lower crust. For abbreviations and location of seismic profiles, see Figure 1a.

Figure 3. Geological map and cross sections of northern Galicia (NW Spain), based on *Martínez Catalán et al*. [2007, 2014]. The scale of the sections is twice that of the map. Red lines in the map mark the location of the geological sections. The rectangle in the map shows the studied area, whose geology is detailed in Figure 5. Section 1 was used to model the Bouguer gravity anomaly (Figures 4b and 7), and its yellow part indicates the location of the magnetic model corresponding to Section D (Figures 10, 11 and 12).

Figure 4. (a) Magnetic anomaly of northern Galicia. Data from the aeromagnetic map of Spain [*Ardizone et al*., 1989], reduced to the pole. Flight lines are shown in white. (b) Bouguer gravity anomaly of northern Galicia. The black line marks Section 1 of Figure 3, modeled as shown in Figure 7. (c) Vertical derivative of the Bouguer gravity anomaly. Contacts and faults are included in (a) and (c) to allow comparison with the geologic map of Figure 3. Rectangles locate the study area.

Figure 5. Geological map of the northern part of the Lugo Dome including the Xistral Tectonic Window. A to D: sections whose magnetic anomaly has been modeled. Coordinates are UTM, Zone 29, in km.

Figure 6. (a) Typical migmatite of the core of the Xistral Tectonic window *c*. 4 km NNE from Viveiro. The melanosome consists of paragneisses derived from the Neoproterozoic Vilalba Series. (b) Detail of the leucosome. Idiomorphic dark dots are magnetite grains. These

contain ilmenite exolved along crystallographic planes and are partially replaced by hematite, mostly along the borders. The pictures depict a large block from the Santa Rosa quarry, 3 km NE of Viveiro (see Figure 5). Rocks in the quarry show magnetic susceptibilities ranging between 0.005 and 0.2 SI.

Figure 7. Model of the Bouguer gravity anomaly along Section 1 (Figures 3 and 4b). Only blocks with significant density contrasts have been modeled. Density in kg m^{-3}. No vertical exaggeration.

Figure 8. (a) Absolute magnetic anomaly map of the Xistral Tectonic Window calculated from 315 ground measurements. (b) Map of the absolute magnetic anomaly reduced to the pole (RTP). (c) Map of geological domains and values of the magnetic susceptibility measured *in situ* and equal or higher than 0.001 SI (values multiplied by 10^3). QTC: Quaternary and Tertiary cover; VGR: Variscan granitoids; OSD: Ollo de Sapo Domain; MND: Mondoñedo Nappe Domain; XTV: Xistral Tectonic Window. (d) Vertical derivative of the Bouguer gravity anomaly map for the same area. Contacts and faults included to allow comparison with the geologic map of Figure 5.

Figure 9. (a) Upward continuation to 3000 m above sea level of the magnetic anomaly acquired at ground level. (b) Detail of the aeromagnetic anomaly [data from *Ardizone et al*., 1989], for the Xistral Tectonic Window area. Contacts and faults are included.

Figure 10. 2D models of the magnetic anomaly in four sections across the Xistral Tectonic Window. Only induced magnetization is considered. For modeling, the ground-based anomaly (dots) was used, but the anomaly reduced to the pole is also shown (grey line).The Bouguer gravity anomaly is shown but is not modeled. The model blocks are bounded by a red line, and the magnetic susceptibility (κ, SI) used for each of them is indicated. For legend of lithology and stratigraphy of the geological sections, see Figure 5.

Figure 11. 2D models of the magnetic anomaly in four sections across the Xistral Tectonic Window, including induced and remanent magnetizations. Two models of Section A with different values for M_r are shown. The model blocks are bounded by a red line, and the magnetic susceptibility (κ, SI), and magnetic remanence (A m^{-1}, inclination and declination), used for each of them are indicated. Legend of the geological sections as in Figure 5.

Figure 12. Block distribution resulting from 2D models of the magnetic anomaly in the four sections of Figures 10 and 11 shown in grey shades. Darker grey represents higher magnetic susceptibilities. The figure intends to allow comparison among models that include only induced magnetization (a) and those that also consider remanent magnetization (b).

Figure 13. Radially averaged power spectra and depth estimates of the sources of magnetic anomalies. (a) Data from the ground-based magnetic anomaly of the Xistral Tectonic Window. (b) Data from the whole Eastern Galicia Magnetic Anomaly. In both cases, three slopes, corresponding to deep (red), intermediate (green) and shallow (blue) sources have

been traced. The values in axes horizontal (wave number) and vertical (interval of ln Power) are used to calculate de slopes, which divided by 4π yield the corresponding depths in km.

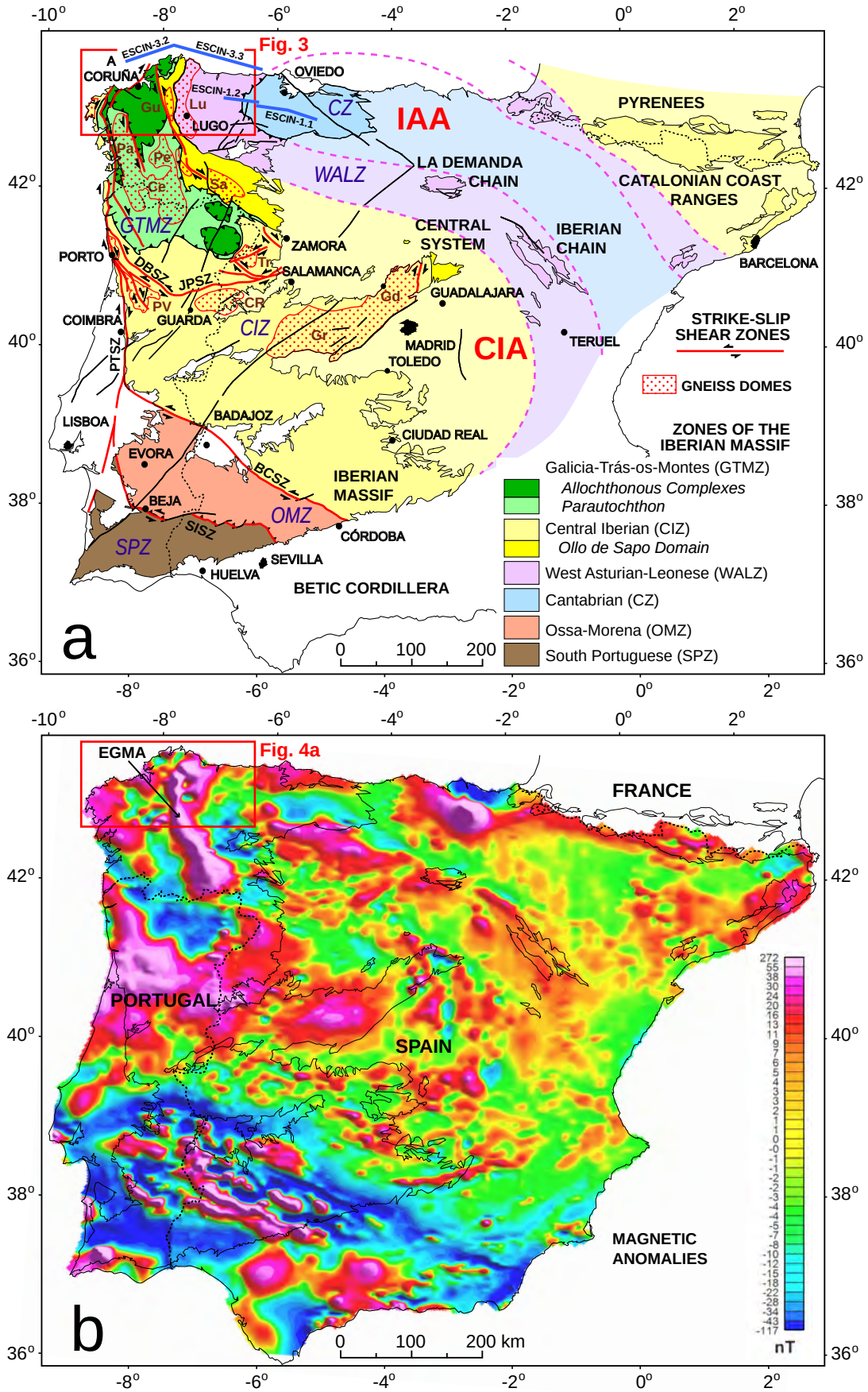
Fig. 3
ESCIN-3.2
ESCIN-3.3
ESCIN-1.2
ESCIN-1.1
A CORUÑA
OVIEDO
LUGO
Gu
Lu
Pa
Pe
Ce
Sa
Tr
CZ
IAA
WALZ
GTMZ
CIZ
CIA
LA DEMANDA CHAIN
CENTRAL SYSTEM
IBERIAN CHAIN
PYRENEES
CATALONIAN COAST RANGES
ZAMORA
SALAMANCA
GUADALAJARA
Gd
Gr
CR
PV
PORTO
DBSZ
JPSZ
COIMBRA
GUARDA
PTSZ
MADRID
TOLEDO
TERUEL
BARCELONA
LISBOA
BADAJOZ
CIUDAD REAL
EVORA
BCSZ
IBERIAN MASSIF
BEJA
OMZ
SISZ
SPZ
CÓRDOBA
SEVILLA
HUELVA
BETIC CORDILLERA
STRIKE-SLIP SHEAR ZONES
GNEISS DOMES
ZONES OF THE IBERIAN MASSIF
Galicia-Trás-os-Montes (GTMZ)
Allochthonous Complexes
Parautochthon
Central Iberian (CIZ)
Ollo de Sapo Domain
West Asturian-Leonese (WALZ)
Cantabrian (CZ)
Ossa-Morena (OMZ)
South Portuguese (SPZ)
a
0 100 200
-10º -8º -6º -4º -2º 0º 2º
42º 40º 38º 36º
EGMA
Fig. 4a
FRANCE
PORTUGAL
SPAIN
MAGNETIC ANOMALIES
nT
b
0 100 200 km

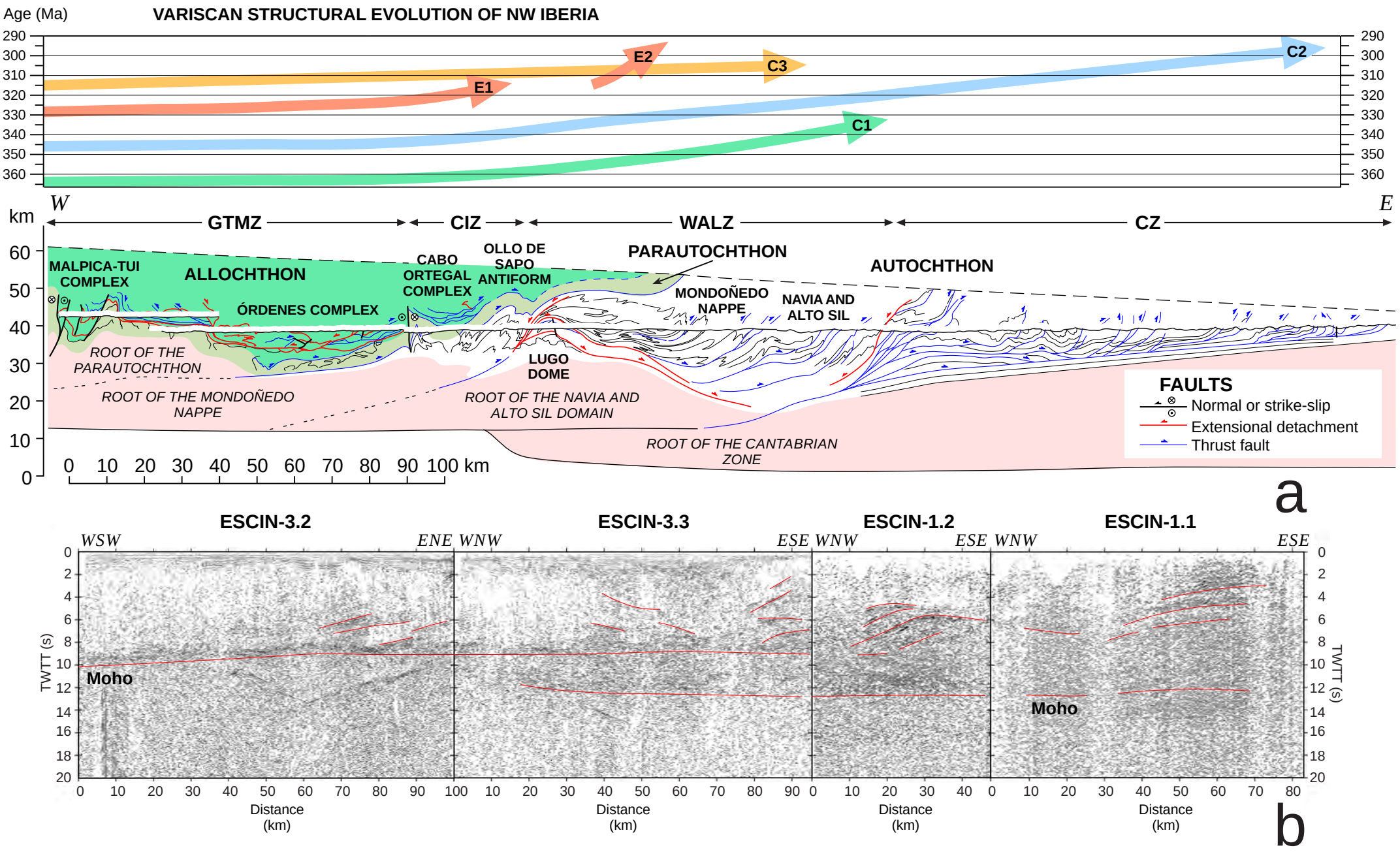
Age (Ma)
VARISCAN STRUCTURAL EVOLUTION OF NW IBERIA
290
300
310
320
330
340
350
360
E1
E2
C3
C2
C1
W
E
km
GTMZ
CIZ
WALZ
CZ
MALPICA-TUI COMPLEX
ALLOCHTHON
ÓRDENES COMPLEX
CABO ORTEGAL COMPLEX
OLLO DE SAPO ANTIFORM
PARAUTOCHTHON
AUTOCHTHON
MONDOÑEDO NAPPE
NAVIA AND ALTO SIL
ROOT OF THE PARAUTOCHTHON
ROOT OF THE MONDOÑEDO NAPPE
LUGO DOME
ROOT OF THE NAVIA AND ALTO SIL DOMAIN
ROOT OF THE CANTABRIAN ZONE
FAULTS
Normal or strike-slip
Extensional detachment
Thrust fault
0 10 20 30 40 50 60 70 80 90 100 km
a
ESCIN-3.2
ESCIN-3.3
ESCIN-1.2
ESCIN-1.1
WSW
ENE WNW
ESE WNW
ESE WNW
ESE
TWTT (s)
Moho
Distance (km)
b

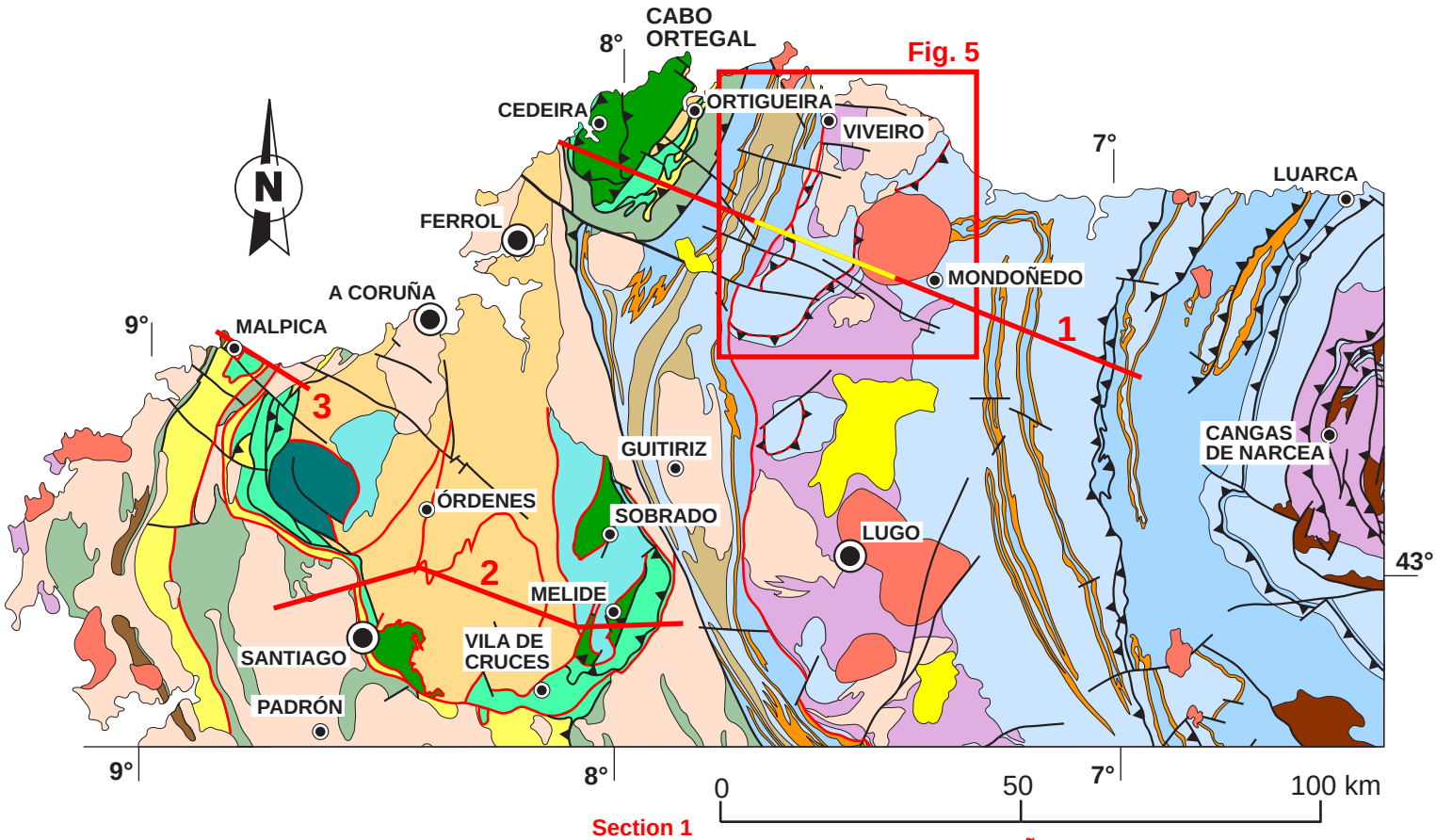

Section 1
CABO ORTEGAL COMPLEX, OLLO DE SAPO ANTIFORM, LUGO DOME AND MONDOÑEDO NAPPE

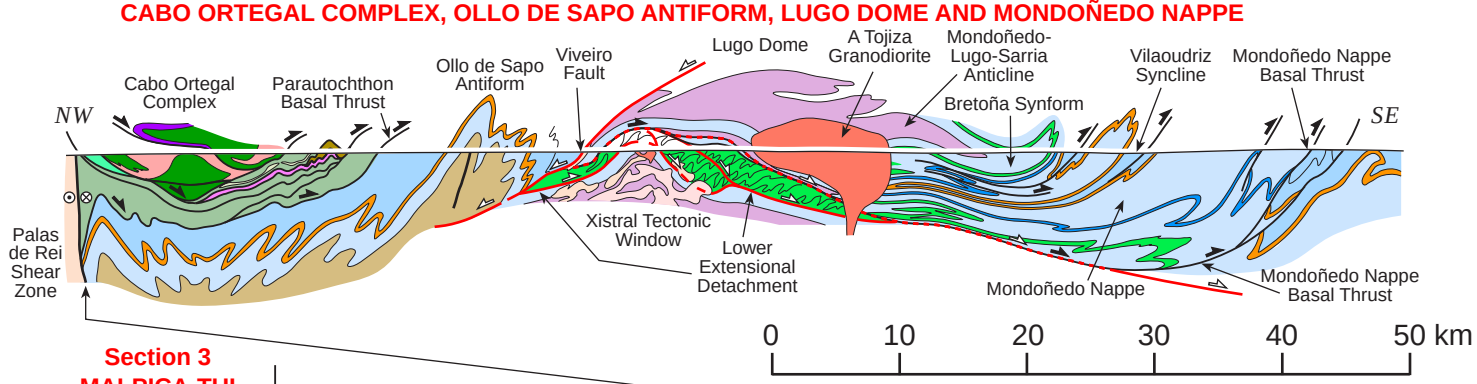

Section 3
MALPICA-TUI COMPLEX

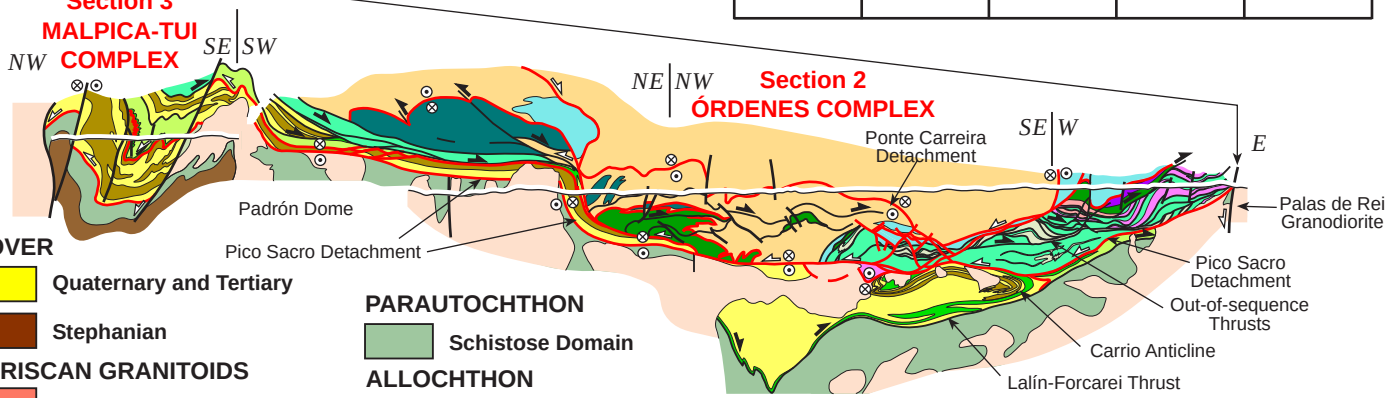

COVER
- Quaternary and Tertiary
- Stephanian

VARISCAN GRANITOIDS
- Postkinematic
- Synkinematic, including migmatitic complexes

AUTOCHTHON
- Middle Ordovician to Devonian
- Armorican Quartzite
- Cambrian-Lower Ordovician
  - Ollo de Sapo Fm.
  - Vegadeo Limestone
  - Upper Cándana-Xistral Qtzte.
- Cambro-Ordovician orthogneisses
- Neoproterozoic (Ediacaran)

PARAUTOCHTHON
- Schistose Domain

ALLOCHTHON

UPPER ALLOCHTHON: IP UNITS
- Metasediments
- Cambro-Ordovician orthogneisses
- Pre-Variscan metagabbros

UPPER ALLOCHTHON: HP-HT UNITS
- Eclogites, mafic granulites and amphibolites
- Metasediments
- Ultramafics

MIDDLE ALLOCHTHON: OCEANIC UNITS
- Metagabbros and amphibolites
- Ultramafics
- Metasediments

LOWER ALLOCHTHON
- Metasediments
- Cambro-Ordovician orthogneisses
- Amphibolites

STRUCTURES
- Normal or wrench fault (map)
- Normal or wrench fault (sections)
- Thrust fault (map)
- Thrust fault (sections)
- Reactivated thrust fault
- Extensional detachment

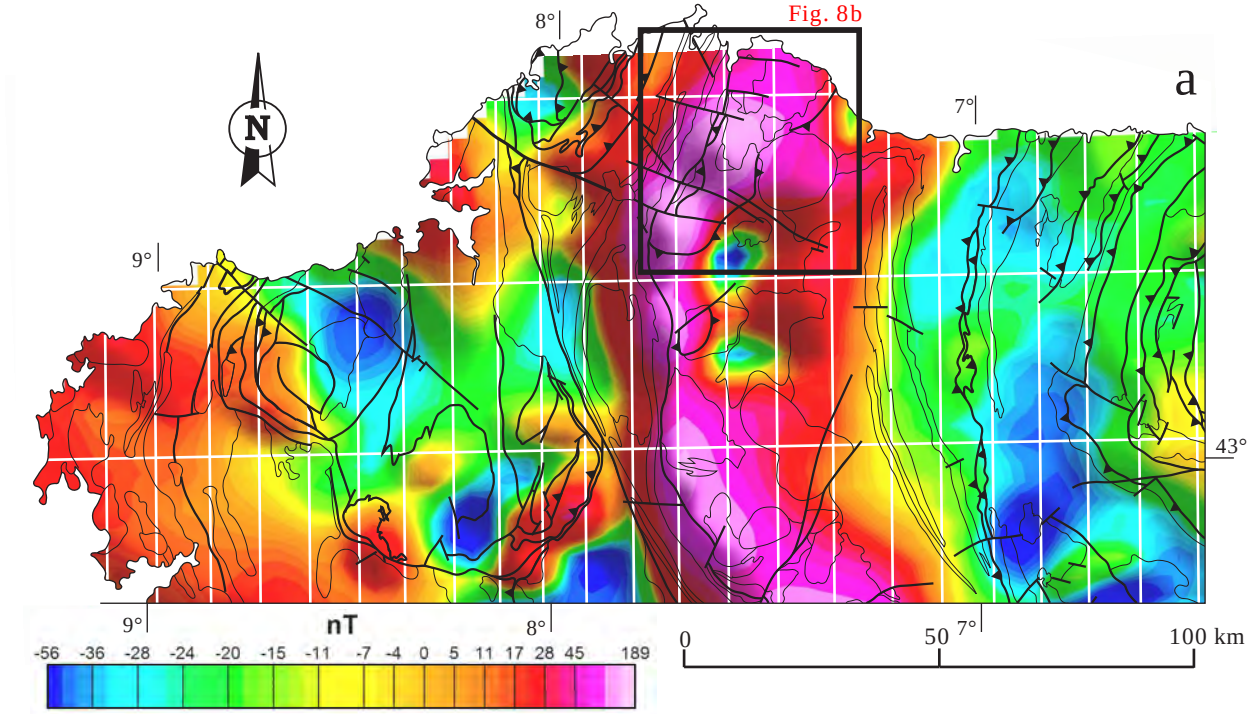
Fig. 8b
a
N
8°
7°
9°
43°
nT
-56 -36 -28 -24 -20 -15 -11 -7 -4 0 5 11 17 28 45 189
0
50
100 km

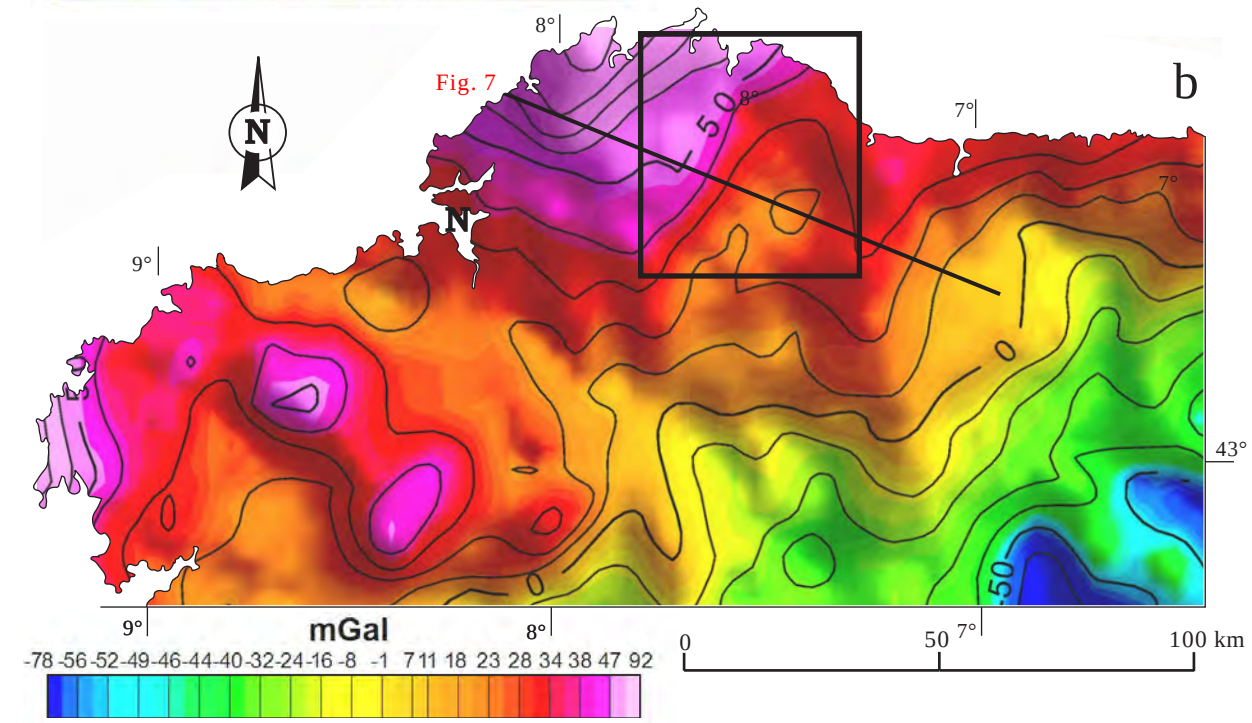
Fig. 7
b
N
8°
7°
9°
43°
50
0
-50
mGal
-78 -56 -52 -49 -46 -44 -40 -32 -24 -16 -8 -1 7 11 18 23 28 34 38 47 92
0
50
100 km

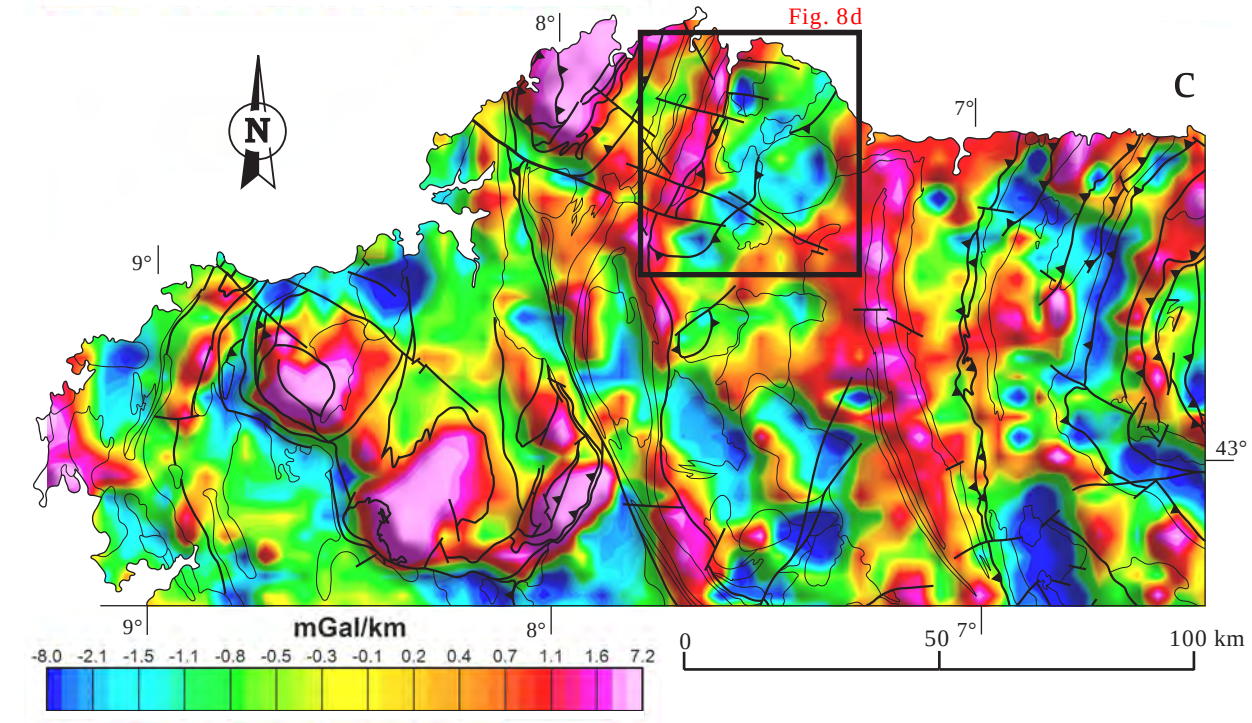
Fig. 8d
c
N
8°
7°
9°
43°
mGal/km
-8.0 -2.1 -1.5 -1.1 -0.8 -0.5 -0.3 -0.1 0.2 0.4 0.7 1.1 1.6 7.2
0
50
100 km

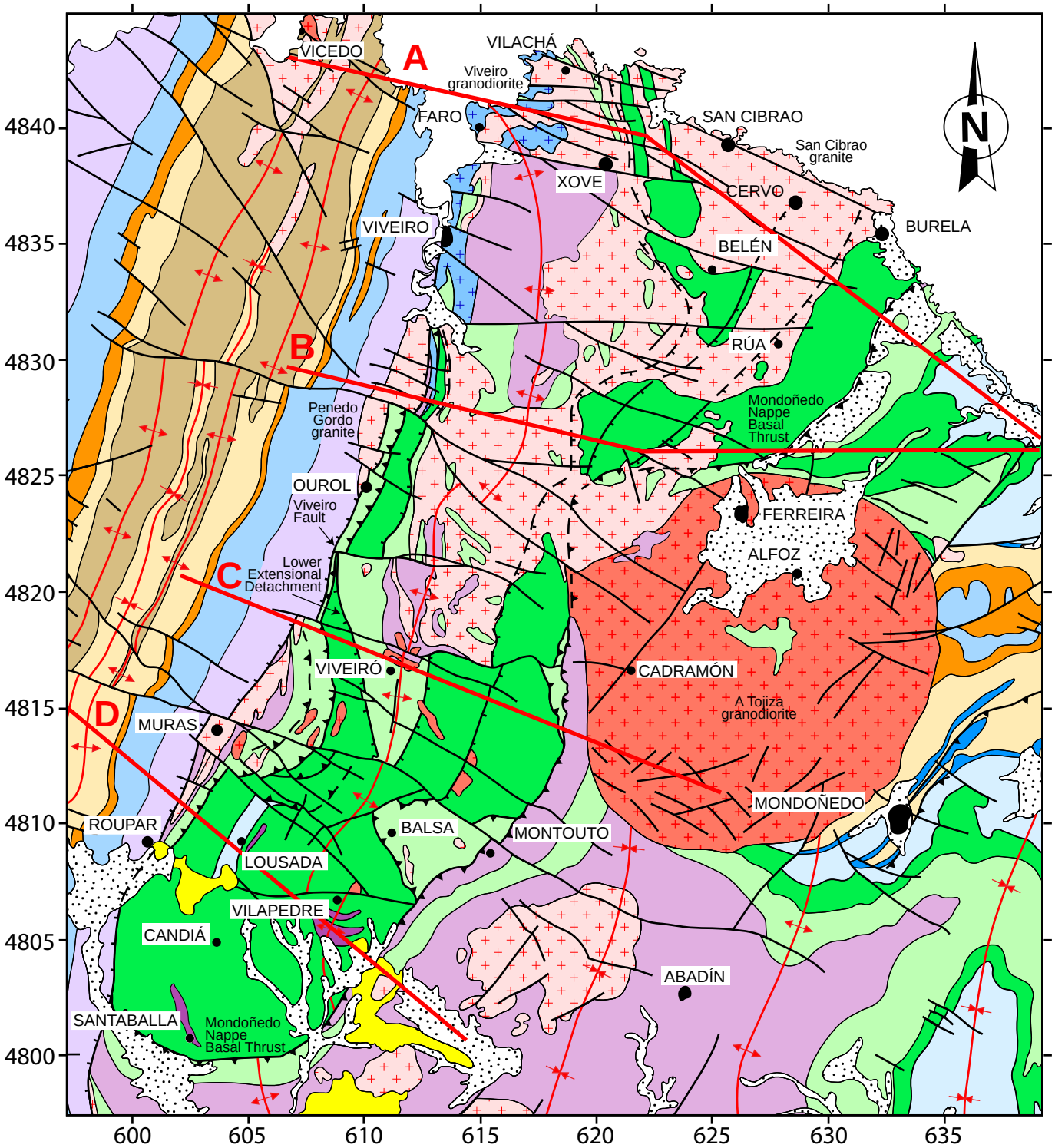

STRUCTURES

- Antiform
- Synform
- High-angle fault
- Extensional detachment
- Thrust fault

COVER

- Quaternary
- Tertiary

VARISCAN GRANITOIDS

- Postkinematic granodiorite
- Syn- and post-kinematic granites
- Synkinematic granodiorite

PALEOZOIC AND NEOPROTEROZOIC

- Slates and carbonaceous slates SILURIAN
- Luarca Slates MIDDLE AND UPPER ORDOVICIAN
- Armorican Quartzite LOWER ORDOVICIAN
- Cabos Group LOWER ORDOVICIAN-UPPER AND MIDDLE CAMBRIAN
- Ollo de Sapo Fm. LOWER ORDOVICIAN
- Vegadeo Limestone MIDDLE-LOWER CAMBRIAN
- Transition Beds LOWER CAMBRIAN
- Upper Cándana and Xistral Quartzites (a: amphibolites) LOWER CAMBRIAN
- Cándana Slates and Lower Cándana Quartzite LOWER CAMBRIAN
- Vilalba Series NEOPROTEROZOIC


a


b

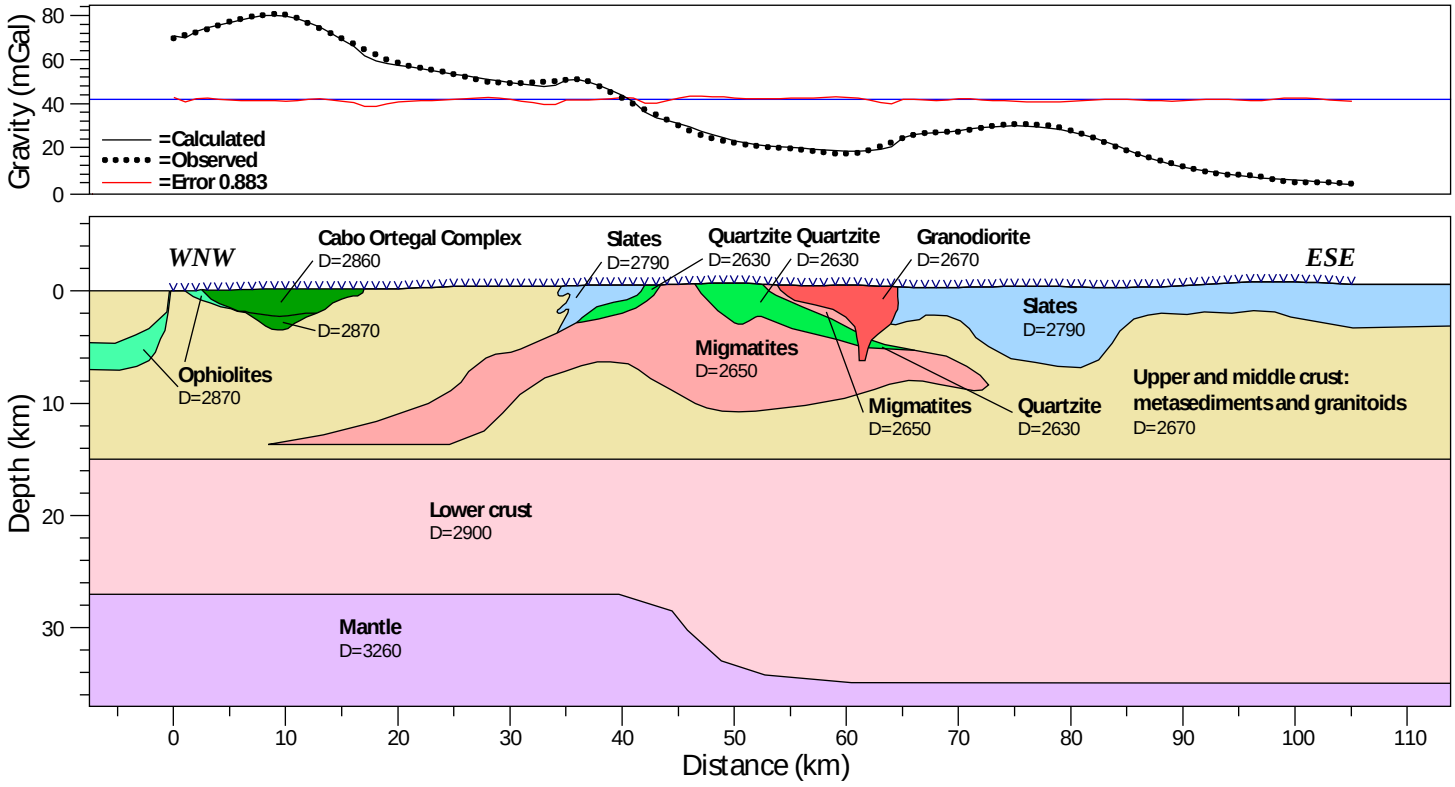
Gravity (mGal)
80
60
40
20
0
=Calculated
=Observed
=Error 0.883
WNW
ESE
Cabo Ortegal Complex
D=2860
D=2870
Ophiolites
D=2870
Slates
D=2790
Quartzite Quartzite
D=2630
D=2630
Granodiorite
D=2670
Migmatites
D=2650
Migmatites
D=2650
Quartzite
D=2630
Slates
D=2790
Upper and middle crust:
metasediments and granitoids
D=2670
Lower crust
D=2900
Mantle
D=3260
Depth (km)
0
10
20
30
0
10
20
30
40
50
60
70
80
90
100
110
Distance (km)

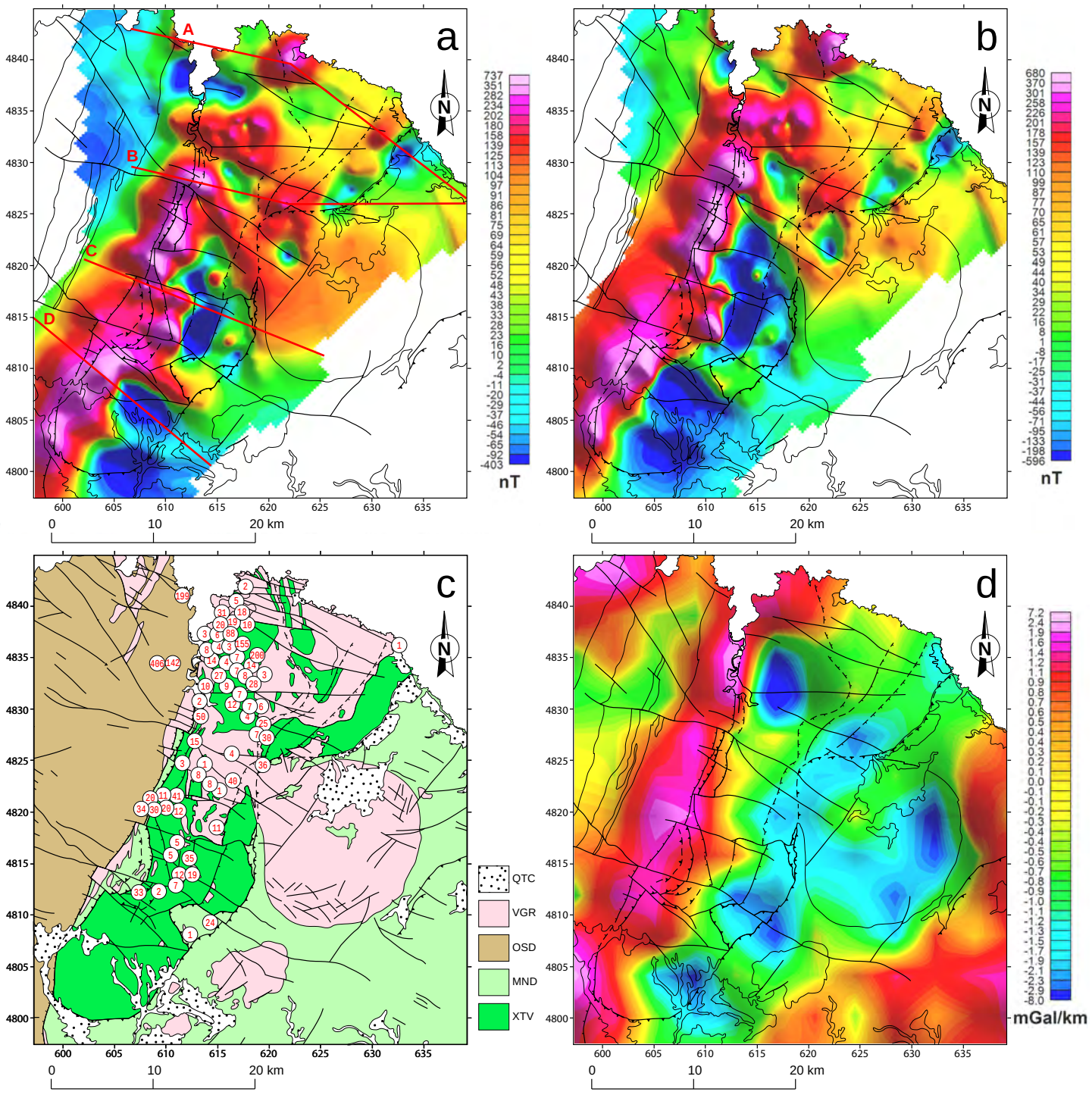
a
b
c
d
A
B
C
D
N
nT
mGal/km
QTC
VGR
OSD
MND
XTV
0
10
20 km

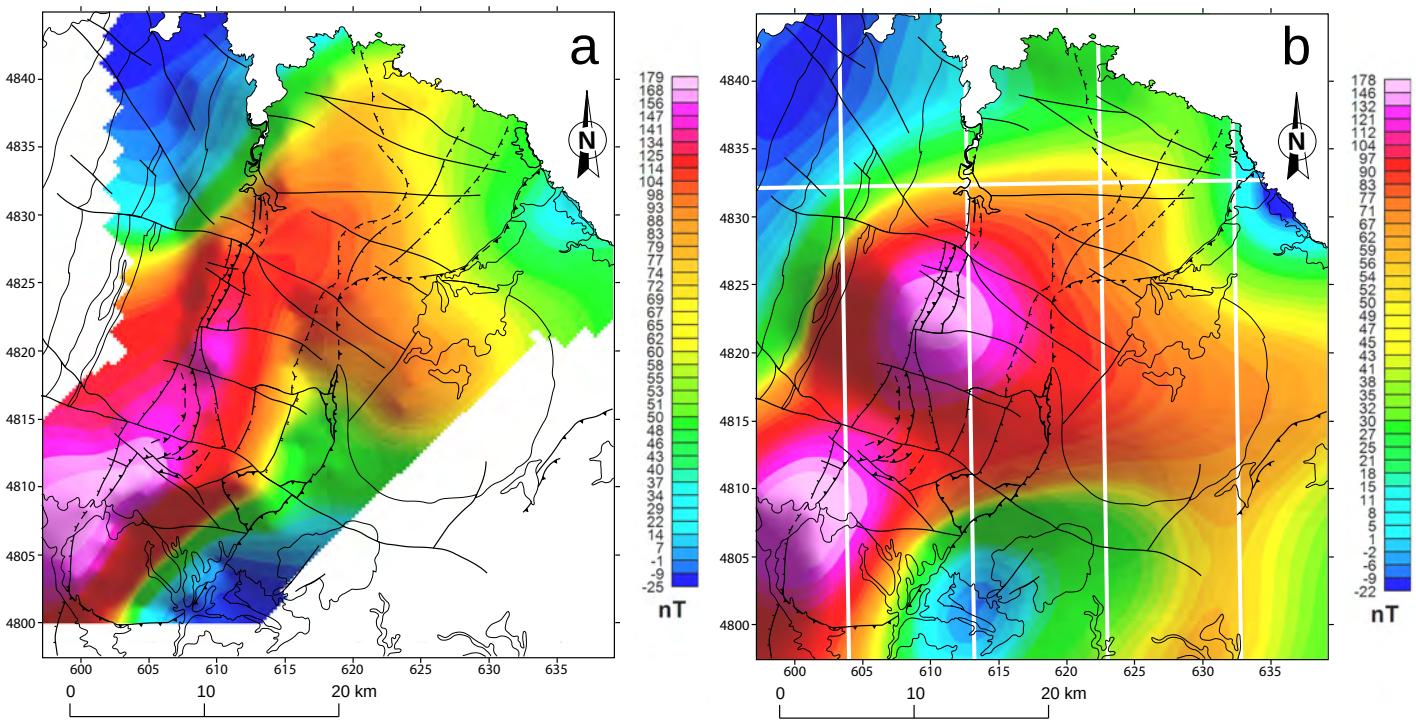
a
b
N
4840
4835
4830
4825
4820
4815
4810
4805
4800
600
605
610
615
620
625
630
635
0
10
20 km
179
168
156
147
141
134
125
114
104
98
93
88
83
79
77
74
72
69
67
65
62
60
58
55
53
51
50
48
46
43
40
37
34
29
22
14
7
-1
-9
-25
nT
178
146
132
121
112
104
97
90
83
77
71
67
62
59
56
54
52
50
49
47
45
43
41
38
35
32
30
27
25
21
18
15
11
8
5
1
-2
-6
-9
-22
nT

Section A

Magnetics (nT)

=Observed
=Error 2.894
=RTP

Grav. (mGal)

=Observed

Depth (km)

WNW
ESE
NW
SE
Ironstone k=0.08
Ironstone k=0.04
Lower extensional shear zone k=0.04
Detachment k=0.04
Detachment k=0.04
Viveiro shear zone k=0.06
Migmatites k=0.02

Section B

Magnetics (nT)

=Calculated
=Observed
=Error 3.408
=RTP

Grav. (mGal)

=Observed

Depth (km)

WNW
ESE
W
E
Detachment k=0.02
Detachment k=0.04
Viveiro shear zone k=0.06
Migmatites k=0.02
Lower extensional shear zone k=0.04

Section C

Magnetics (nT)

=Calculated
=Observed
=Error 3.681
=RTP

Grav. (mGal)

=Observed

Depth (km)

WNW
Viveiro shear zone k=0.06
k=0.06
k=0.06
Lower extensional shear zone k=0.04
Detachment k=0.02
ESE
Granodiorite k=0.001
Viveiro shear zone k=0.08
Migmatites k=0.02

Section D

Magnetics (nT)

=Calculated
=Observed
=Error 4.915
=RTP

Grav. (mGal)

=Observed

Depth (km)

NW
Lower extensional shear zone k=0.04
SE
Detachment k=0.02
Viveiro shear zone k=0.08
Migmatites k=0.02

Distance (km)

STRUCTURES

Fault
Extensional detachment
Thrust fault
Foliation

Section A (1)

=Calculated
=Observed
=Error 5.968
=RTP

Magnetics (nT)

Depth (km)

Ironstone
k=0.084
Mr=1.944, I=-61°, D=162°

WNW

Ironstone
k=0.042
Mr=0.972, I=-61°, D=162°

ESE

NW

Lower extensional shear zone
k=0.084
Mr=1.944, I=-61°, D=162°

Detachment
k=0.084
Mr=1.944, I=-61°, D=162°

SE

Detachment
k=0.042
Mr=0.972, I=-61°, D=162°

Viveiro shear zone
k=0.084
Mr=1.944, I=-61°, D=162°

Migmatites
k=0.021
Mr=0.486, I=-61°, D=162°

Section A (2)

=Calculated
=Observed
=Error 4.409
=RTP

Magnetics (nT)

Depth (km)

Ironstone
k=0.08
Mr=1.602, I=-28°, D=156°

WNW

Ironstone
k=0.04
Mr=1.068, I=-28°, D=156°

ESE

NW

Lower extensional shear zone
k=0.06
Mr=1.602, I=-28°, D=156°

Detachment
k=0.06
Mr=1.602, I=-28°, D=156°

SE

Detachment
k=0.04
Mr=1.068, I=-28°, D=156°

Viveiro shear zone
k=0.04
Mr=1.068, I=-28°, D=156°

Migmatites
k=0.02
Mr=0.534, I=-28°, D=156°

Section B

=Calculated
=Observed
=Error 4.784
=RTP

Magnetics (nT)

Depth (km)

WNW

ESE

W

Detachment
k=0.04
Mr=1.068, I=-28°, D=156°

Detachment
k=0.02
Mr=0.534, I=-28°, D=156°

E

Viveiro shear zone
k=0.08
Mr=2.136, I=-28°, D=156°

Migmatites
k=0.02
Mr=0.534, I=-28°, D=156°

Lower extensional shear zone
k=0.04
Mr=1.068, I=-28°, D=156°

Section C

=Calculated
=Observed
=Error 3.618
=RTP

Magnetics (nT)

Depth (km)

WNW

k=0.06
Mr=1.602, I=-28°, D=156°

k=0.06
Mr=1.602, I=-28°, D=156°

Lower extensional shear zone
k=0.04
Mr=1.068, I=-28°, D=156°

ESE

Granodiorite
k=0.001
Mr=0.027, I=-28°, D=156°

Viveiro shear zone
k=0.06
Mr=1.602, I=-28°, D=156°

Detachment
k=0.03
Mr=0.801, I=-28°, D=156°

Migmatites
k=0.02
Mr=0.534, I=-28°, D=156°

Section D

=Calculated
=Observed
=Error 3.965
=RTP

Magnetics (nT)

Depth (km)

NW

Lower extensional shear zone
k=0.04
Mr=1.068, I=-28°, D=156°

Detachment
k=0.04
Mr=1.068, I=-28°, D=156°

SE

Viveiro shear zone
k=0.08
Mr=2.136, I=-28°, D=156°

Migmatites
k=0.02
Mr=0.534, I=-28°, D=156°

Distance (km)

STRUCTURES

Fault

Extensional detachment

Thrust fault

Foliation

MODELS USING MAGNETIC SUSCEPTIBILITY

MODELS INCLUDING MAGNETIC REMANENCE

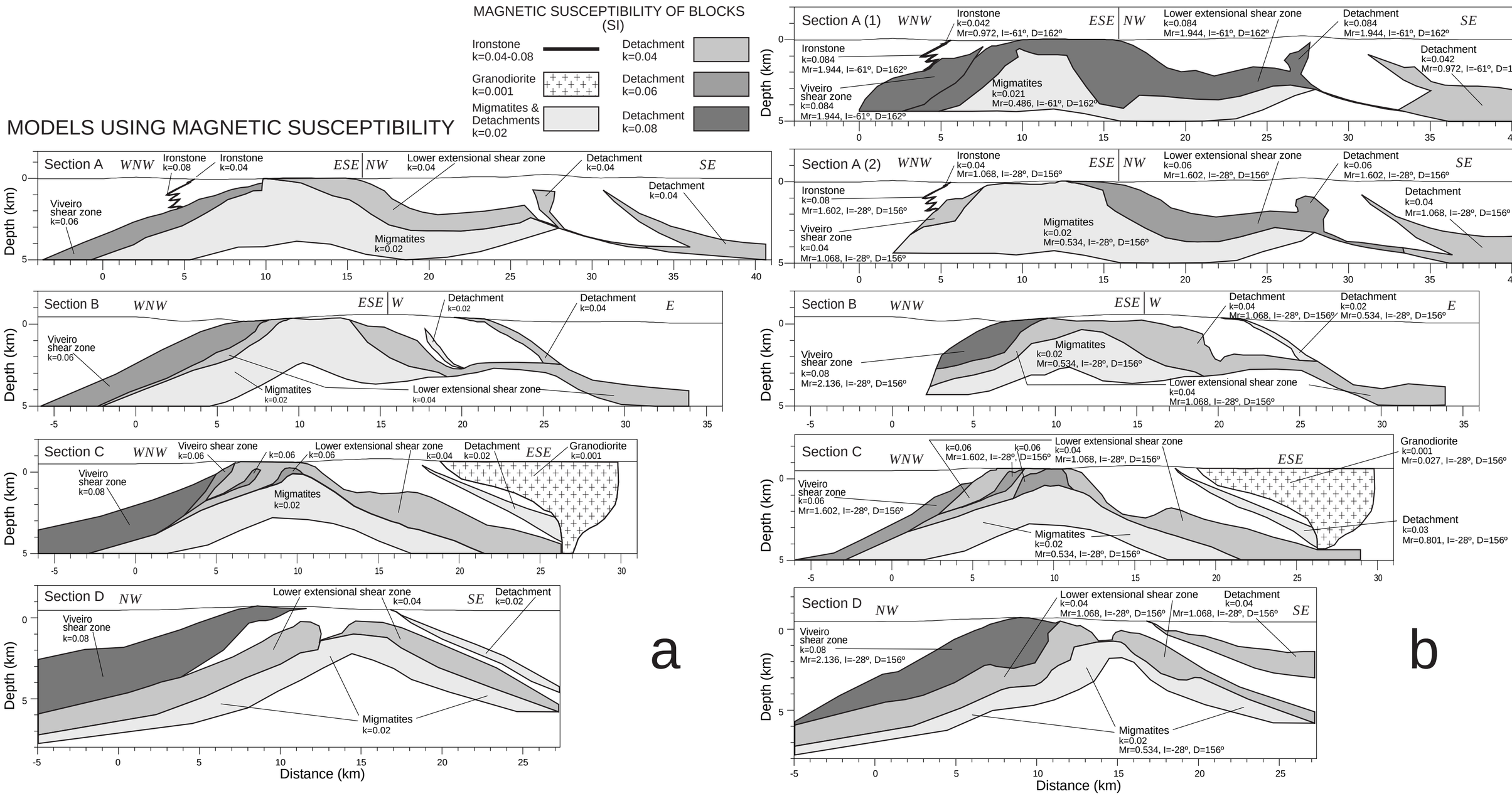

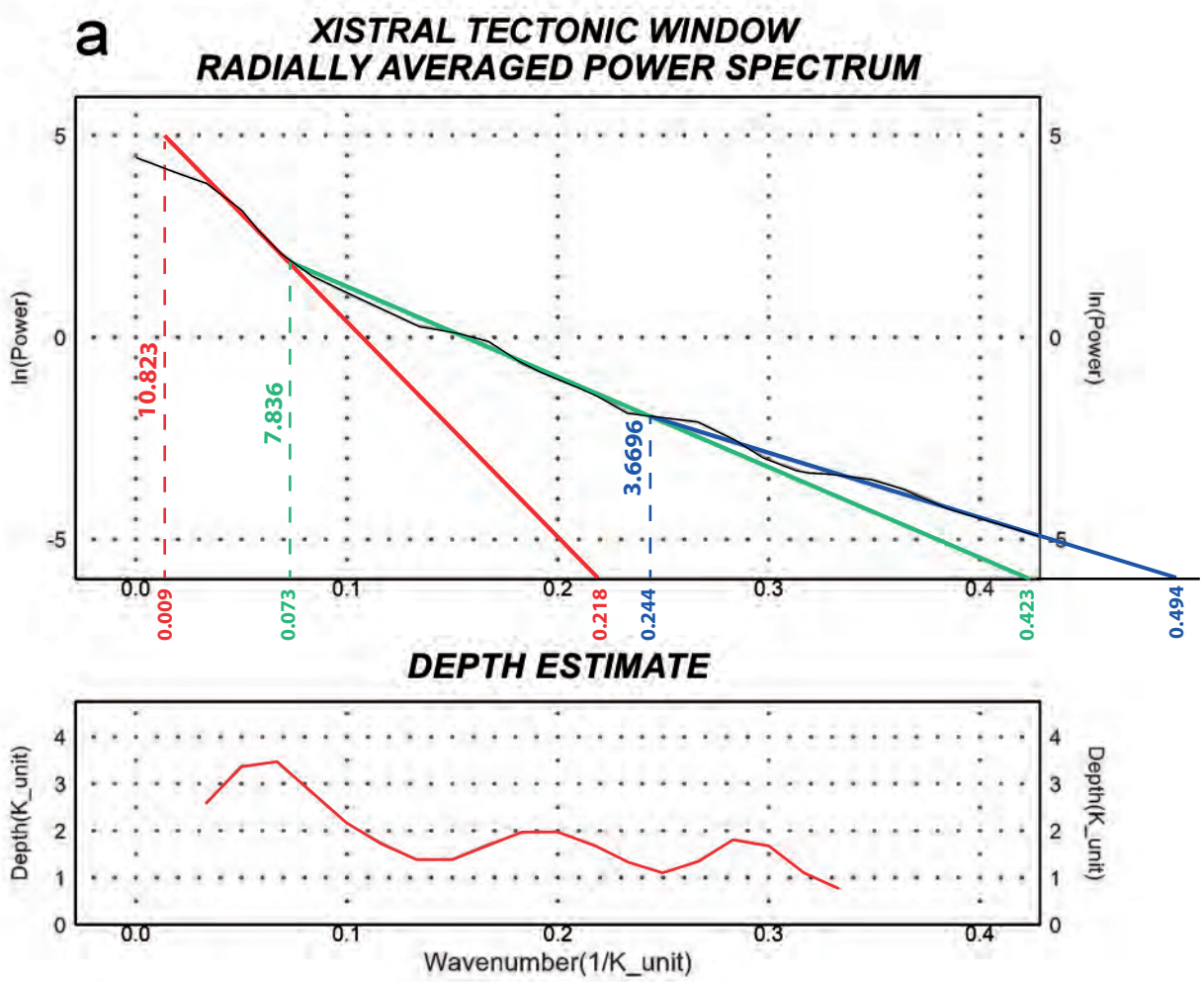
a
XISTRAL TECTONIC WINDOW
RADIALLY AVERAGED POWER SPECTRUM
ln(Power)
10.823
7.836
3.6696
0.009
0.073
0.218
0.244
0.423
0.494
DEPTH ESTIMATE
Depth(K_unit)
Wavenumber(1/K_unit)

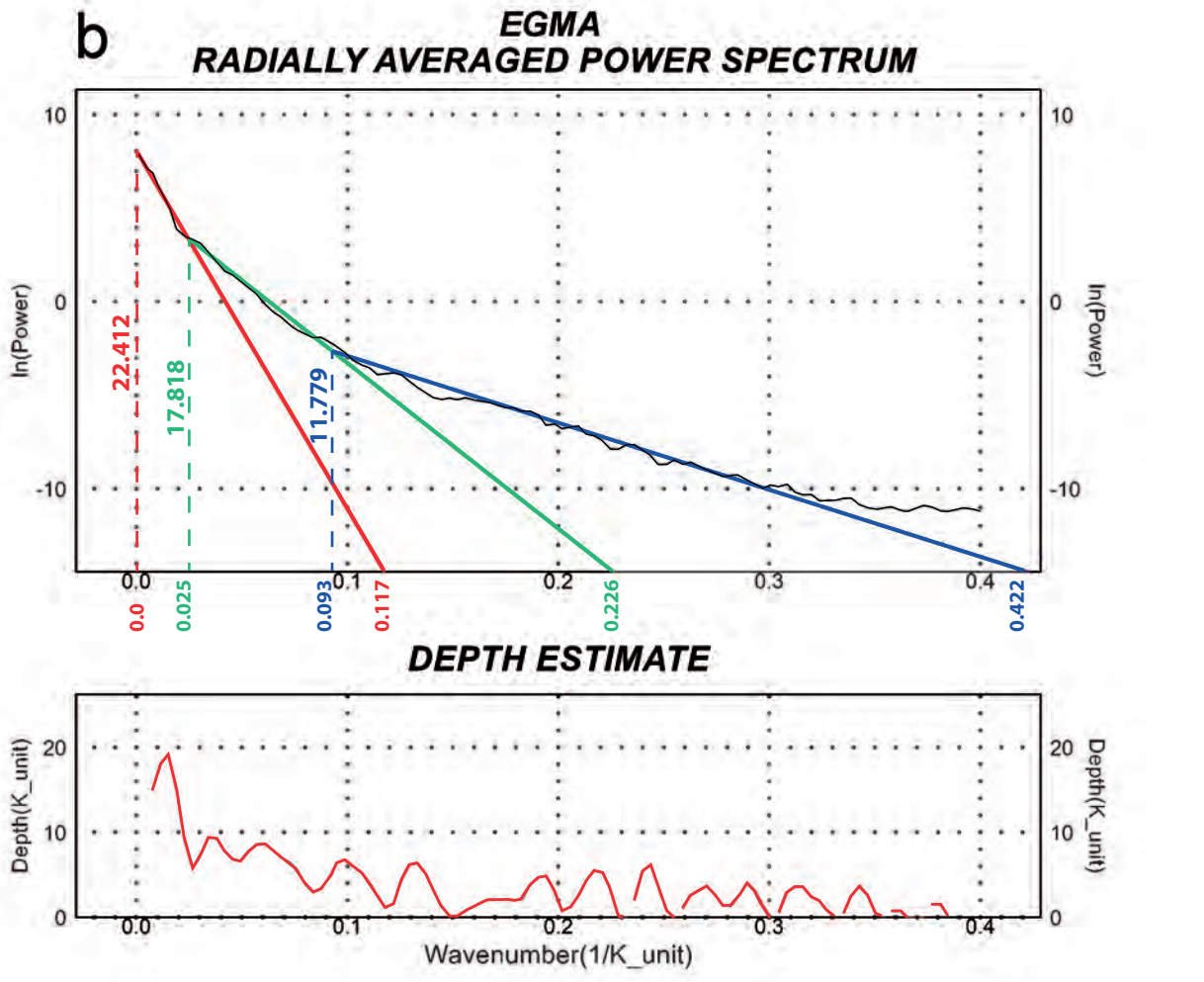
b
EGMA
RADIALLY AVERAGED POWER SPECTRUM
ln(Power)
22.412
17.818
11.779
0.0
0.025
0.093
0.117
0.226
0.422
DEPTH ESTIMATE
Depth(K_unit)
Wavenumber(1/K_unit)